Sniffing Trees:
A UAV Based Photoionization Detector for Biogenic Volatile Organic Compound Emission Measurements

A Thesis Presented

by

Vladislav I. Sevostianov

to

The Department of Earth and Planetary Sciences,
The Department of Mathematics, and
The Global Health and Health Policy Secondary Field
in partial fulfillment of the requirements
for a degree with honors
of Bachelor of Arts

November 2019
Harvard College

ABSTRACT

For practical use in forecasting weather and understanding climate, global climate models rely on global emission models, such as the Model of Emissions of Gases and Aerosols from Nature (MEGAN), which rely on accurate emission inventories. Standard approaches in atmospheric sciences for emissions measurement, such as ground tower observations, aircraft flybys, and satellite measurements are all inadequate for high resolution, accurate estimates from biogenic sources. Measurements from unmanned aerial vehicles (UAVs) allow for very high-resolution atmospheric data collection across an area, taking into account the vast plant diversity within an area such as the Amazon. Volatile Organic Compounds (VOCs), well-known for their central role in air pollution formation, are of interest in ecosystem functioning, atmospheric chemistry, and climate change. Isoprene, a secondary metabolite of photosynthesis, is typically of chief interest and has a relatively long lifetime in the atmosphere. Other larger compounds with shorter lifetimes, such as diterpenes, may not be fully accounted for in current measurements. Current methodologies do not allow for dynamic, real-time, and high-resolution measurements, and additionally, there are numerous issues for instruments measuring VOCs such as sensitivity, low portability, and slow response times.

To address these deficiencies, a custom-built, highly sensitive photoionization detector (PID) operating in real-time is designed and mounted on a UAV. Photoionization detectors are some of the only ways to simultaneously address sensitivity, portability, and rapid response time in a single system, yet commercial sensors face a 1 ppb resolution barrier which is insufficient for measurements of many biogenic VOCs. The sensor is tested, calibrated, and evaluated using laboratory studies. The PID estimates the total concentration of all VOCs in its operating range, and functions as a proxy measurement for total VOC concentration based on the operationalized definition of isoprene equivalent concentration. Through onboard data transmission, determination of so called “super emitters” amongst heterogeneous biogenic sources is possible. Additionally, through real-time measurement it is possible to correlate chemical emissions with fluctuations from meteorological variables, and it becomes possible to evaluate multiple locations quickly and assess emission events with better clarity. Furthermore, this may provide insights into the effects of induced environmental stresses upon biogenic systems, the dynamics of which are still not fully understood.

TABLE OF CONTENTS

LIST OF FIGURES

LIST OF TABLES

ACKNOWLEDGMENTS

Professor Scot Martin (Harvard University)
Matthew Stewart (Harvard University)
Dr. Jianhuai Ye (Harvard University)
Other Members of the Martin Research Group
Maddie Hickman, Steve Cortesa, Elaine Kristant, Evan Smith (Harvard Active Learning Labs)
Andy DiMambro, Steve Sansone, Stan Cotreau, (Harvard Physics Machine Shop)
Jim MacArthur, Mike Litchfield (Harvard Physics Electronics Shop)
Dr. Annika Quick and Dr. Esther James (Harvard University)
Harvard University Earth and Planetary Sciences Department
Harvard University Statistics Department
Harvard University Center for the Environment Research Grant, 2019
Harvard University Earth and Planetary Sciences Undergraduate Research Grant, 2019
Friends & Family

1. INTRODUCTION

1.1 Motivation and General Statement of Problem

The purpose of this research was to develop a sensor for higher spatiotemporal resolution of biogenic emissions of volatile organic compounds (VOCs). Currently, several standard approaches are used: monitoring towers, aircraft flybys, and satellite measurements (Koppmann, 2007; Villa, Gonzalez, *et al.*, 2016). However, all of these methods have disadvantages that can be addressed through the use of unmanned aerial vehicles (UAVs), also known as drones (Villa, Gonzalez, *et al.*, 2016; Jacob *et al.*, 2018). While tower measurements allow for very accurate measurements in a particular region, they are not mobile, and thus cannot necessarily give an accurate sampling representation if they are in an heterogeneous area (such as a natural forest) (Petrokofsky *et al.*, 2012; Haszpra *et al.*, 2015). Aircraft (and satellite) measurements allow for mobility, though due to the speed of collection in flight, individual measurements tend to be blurred together and consequently there is very poor resolution (Guimaraes *et al.*, 2019). UAV measurements allow for very high resolution across an area, taking into account the vast biotic variation within an area such as the Amazon (Villa, Gonzalez, *et al.*, 2016). The Amazon contains 390 billion trees and 16,000 tree species, dominated by around 200 tree species, and the different forest subtypes and altitude may influence local emissions due to the differing plant life and fauna found in those areas (ter Steege *et al.*, 2013). VOCs are a key component to aerosol (or particulate matter) and ozone air pollution, and while anthropogenic activities can significantly affect VOC concentrations, they are predominantly produced by plants (Hewitt *et al.*, 1993). As different plants species release different VOCs in different quantities under different conditions, this means there are local

concentration differences that may persist far above where the VOCs are released and consequently, air pollution is heterogeneously produced (Koppmann, 2007). Proper measurements require a UAV-based sensor system that is extremely sensitive and capable of operating at a high response rate to ensure the high spatiotemporal resolution advantage is maintained.

Besides air pollution concerns, a better understanding of biogenic VOC emissions is crucial for accurate regional and global climate models. Models such as MEGAN (Model of Emissions of Gases and Aerosols from Nature), which are used both standalone and as a component of larger models, rely on accurate measurements of plant emissions (Guenther *et al.*, 1995). In much the same way as most vehicle pollution is disproportionally due to a minority of cars (Wang *et al.*, 2015), so too can this be the case with biogenic sources. Thus, these "super-emitting" plants may well be unaccounted for in current models if they happen to be isolated from tower measuring stations. Tower measuring stations are typically built in similar areas, dependent on factors such as soil quality for construction, biasing their locations (Batista *et al.*, 2019).

The dynamics of forest system health and VOC emissions are not fully understood, but changing VOC emission concentrations may be an indicator of water or heat stress and other climate related factors (Holopainen and Gershenzon, 2010; Banerjee and Sharkey, 2014). VOCs can also be used as trace compounds to understand other atmospheric chemical reactions that are not possible to measure directly (Koppmann, 2007).

Additionally, as current UAV-based sampling techniques are not real time, but rather capture the gas and then use laboratory analysis (such as thermal desorption gas chromatography mass spectrometry (TD-GC-MS)), there is a significant time lag between

gas intake and the analysis (Mckinney *et al.*, 2018). This may lead to the possibility of inaccurate data collection as the more volatile compounds with shorter lifetimes could not be fully accounted (Matsumoto, 2014). Globally, carbon sinks do not balance with carbon emissions, and the nature and location of this carbon sink has been the subject of much speculation and debate (Jacob, 1999; Schindler, 1999; Wang *et al.*, 2016). Consequently, it is possible that larger VOCs (such as diterpenes) are part of the "missing carbon" dilemma regarding the global carbon budget (Kesselmeier *et al.*, 2002). First the chemistry of VOCs and their importance will be addressed, followed by design considerations of the sensor.

1.2 VOC Chemistry

1.2.1 Types of VOCs

VOC is an umbrella term for a large class of compounds (Atkinson and Arey, 2003). There are thousands of different types of VOCs, and every country has slightly different definitions (due to VOCs' applications in industry and corresponding environmental regulations). Under the United States' Environmental Protection Agency (EPA), "VOCs are considered to be those organic compounds having a vapor pressure greater than 10 Pa at 25°C, a boiling point of up to 260°C at atmospheric pressure, and 15 or less Carbon atoms" (Koppmann, 2007). Nearly every single activity involving biological organisms releases trace amounts of various organic species to the atmosphere, and VOCs are primarily removed through chemical oxidation by either OH, O_3, NO_3, or halogen radicals, and to a lesser extent through photolysis and deposition (Koppmann, 2007).

1.2.2 Chemical Pathways

VOCs play a role in air pollution formation, particularly of tropospheric ozone and aerosols, which is especially of interest in urban areas (Ioffe, Isidorov and Zenkevich,

1977; Edgerton *et al.*, 1989). Ozone (toxic to life in the troposphere, while very beneficial in blocking UV radiation in the stratosphere) formation occurs under two different regimes: NO_x limited (or VOC saturated) and NO_x saturated (or VOC limited) (Carter, 1994; Jacob, 1999). Ozone formation is demonstrated by the following equations (Jacob, 1999):

(1) $$VOC + OH \rightarrow OPR + H_2O$$

(2) $$OPR + NO \rightarrow OOR + NO_2$$

(3) $$NO_2 + hv \rightarrow NO + O_3$$

These reactions depend on freely available oxygen (O_2) in the atmosphere. Organic peroxyradicals (OPR) can react with NO_x (specifically NO) to form organic oxyradicals (OOR) and NO_2. This completes VOCs' oxidation. Once NO_2 is produced, it easily proceeds to be photolyzed to produce NO and ozone. This may be limited by either the first or second equations; either the initial VOC reaction is what slows everything down, or the secondary OPR and NO reaction does. The rate-controlling reaction determines the ozone formation regime.

At low NO_x concentrations, OPR can react with itself, which produces peroxides. This limits ozone production, and the VOCs have no limiting role. At high NO_x concentrations however, all the VOCs participate in ozone formation and as a result ozone production increases linearly with VOC concentrations (Jacob, 1999).

In addition to their role in ozone and NO_x, VOCs are related to atmospheric aerosol concentrations. While primary organic aerosols (POA) may be released through fuel combustions and forest fires (for example, soot), VOCs are responsible for production of secondary organic aerosols (SOA) (Griffin, Cocker and Seinfeld, 1999). VOCs are oxidized in the atmosphere and form low volatility products (Henze and Seinfeld, 2006).

These are formed from successive oxidation of organic chemicals until their vapor pressure reduces sufficiently to partition partly or solely to the particle phase. Upon condensing, these products then form particulate matter, as observed in pathway 2 of figure 1.1. Globally, between 20% and 90% of fine aerosol (under 1 μm) is organic carbon based (Jimenez *et al.*, 2009). Generally, the larger VOCs (i.e., sesquiterpenes vs terpenes or isoprenoids) yield more SOA per carbon atom (up to 67% more for sesquiterpenes) (Kanakidou *et al.*, 2005) . New detecting capabilities will help quantify VOCs and identify their sources.

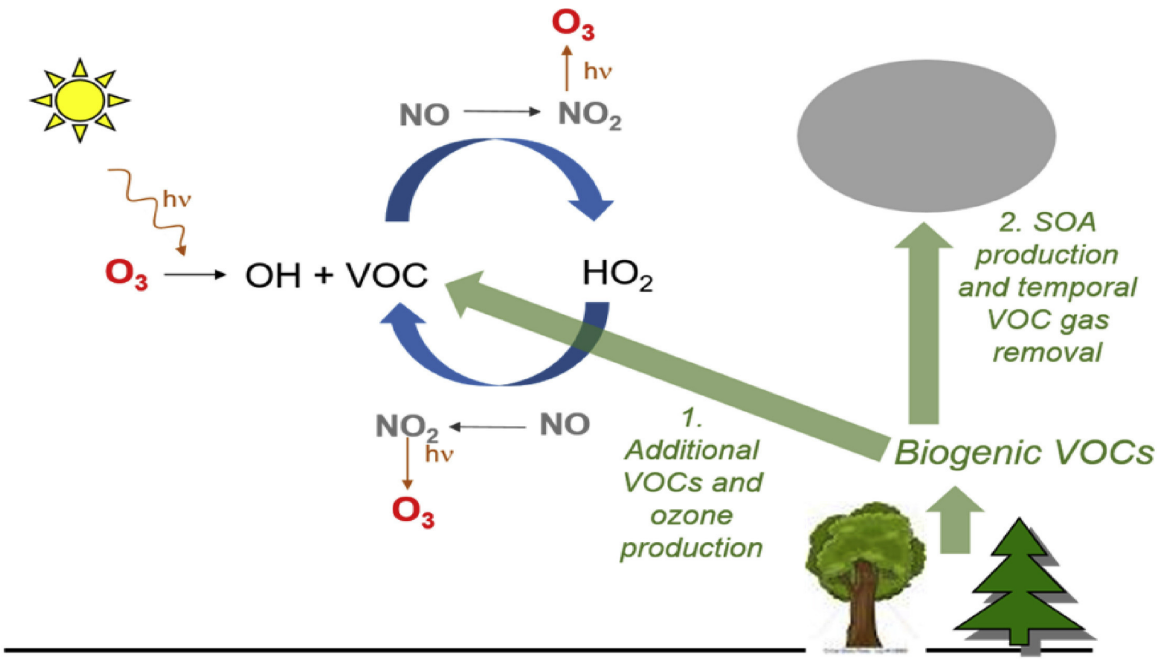

Figure 1.1. VOC chemistry pathway in the atmosphere in the formation of air pollution. From (Bonn et al., 2018)

1.2.3 Biogenic VOC Production and Emission

Biogenic emissions of VOCs are the bulk of all VOC emissions (about 2/3), and the most important biogenically released VOC is isoprene, representing between 30% and 50% of all emissions globally (Koppmann, 2007; Wennberg *et al.*, 2018). Isoprene is typically oxidized within an hour by the OH radical, though some terpene VOCs may be

reactive oxidizers as well (Carlo *et al.*, 2004; Wennberg *et al.*, 2018). While flowers and fruits emit the greatest variety of VOCs, leaves are primarily responsible for most of the emitted mass, with isoprene playing the most important role (Laothawornkitkul *et al.*, 2009).

Isoprene is produced via the methylerythritol 4-phosphate (MEP) pathway in the chloroplasts of many plants as an effective byproduct of photosynthesis (Banerjee and Sharkey, 2014). Typically all the carbon in isoprene comes from the Calvin-Benson cycle which governs CO_2 uptake and metabolization in plants, and thus this cycle also effectively governs isoprene production. (Wennberg *et al.*, 2018). Isoprene production changes are tied to CO_2 input changes, though the exact mechanism is still a matter of debate; however, with more CO_2, the Calvin-Benson cycle typically is more active, leading to more isoprene production. In many plants, isoprene production is significantly reduced or completely stopped in darkness, as the Calvin-Benson process stops cycling. (Banerjee and Sharkey, 2014). This ensures a diurnal cycle of isoprene concentrations. Improving VOC measuring techniques and capabilities will provide a new lens through which other changing factors such as CO_2 can be evaluated.

1.3 Photoionization Detectors

1.3.1 General Principles and Overall Design

In a photoionization detector, a UV lamp shines into a gas chamber and excites the sample (Sevcik, 1976). Being ionized, the electrons and charged molecules are propelled onto detector plates that surround the chamber. These plates pick up the particles and the current that is measured is proportional to the concentration of the ionized particles (RAE Systems, 2013). The energy of the lamp's photons determines which components of the gas sample are ionized; generally, VOCs are more easily ionized than most air molecules,

and so only the VOCs are consequently picked up (table 1) (Sevcik, 1976). In designing the detector, the lamp fill gas, the window material, excitation method, and detector plate design all need to be optimized.

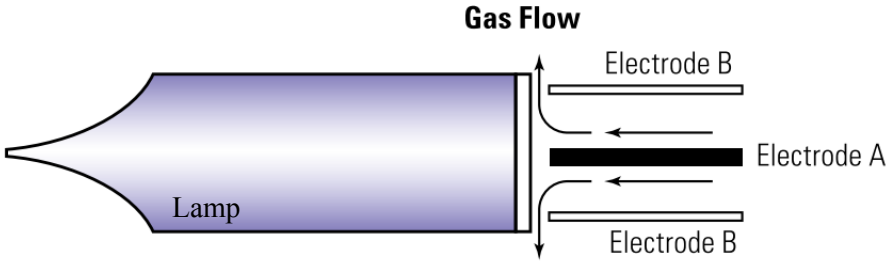

Figure 1.2. General sensor design (RAE Systems, 2013). The gas chamber is the area between the electrodes (detector plates). Gas flow is directed by the pump.

Table 1. Ionization energies of the major components of air (RAE Systems, 2013) (2.3.1).

Gas	Atmospheric Mole Fraction (ppmv)	I.E. (eV)
N_2	780840	15.58
O_2	209460	12.07
Ar	9340	15.76
CO_2	330	13.78
Ne	18.18	21.56
He	5.24	24.59
CH_4	2	12.61
Kr	1.14	14.00
H_2	0.5	15.43
N_2O	0.5	12.89
Xe	0.087	12.13
H_2O	0 – 40000	12.62

Table 2. Select characterizations of some VOCs of interest (Ion Science, 2019)

VOC	I.E. (eV)	Chemical Formula
Isoprene	8.85	C_5H_8
Methanol	10.85	CH_4O
Alpha-Pinene	8.07	$C_{10}H_{16}$
Limonene	8.6	$C_{10}H_{16}$
Myrcene	8.2	$C_{10}H_{16}$
Acetone	9.69	C_3H_6O
Caryophyllene	9.0	$C_{15}H_{24}$

Ionization energy refers to the energy required to remove a valence electron from molecular orbit (Politzer, Murray and Bulat, 2010). As all elements of the air sample with ionization energies below the energy of the lamp may be ionized (if they are hit by a photon), the sensor will measure the total aggregate volatile organic compound concentrations (Devine *et al.*, 2014). While a higher energy will result in a broader sweep in the category of particles targeted, a higher quantity of photons of the same energy will ensure more elements in the samples are effectively measured. It is inevitable, especially at lower concentrations, that some compounds will not be hit by the emitted photons, and so increasing photon flux will increase net sensitivity (Langhorst, 1981).

The wavelength of the produced light determines which VOCs in particular will be detected; by using shorter wavelengths, more stable VOCs can be ionized (as the photons have more energy) and conversely, by using light of longer wavelength, those VOCs may be excluded (Langhorst, 1981). In order to ionize most VOCs, the wavelength needs to be in the vacuum ultra-violet spectrum (VUV). There are several excitation design methods and several bulb gasses that may all be appropriate. Table 3 lists some possible gases that may be used in the UV bulb.

Table 3. Different excitation gases to be used in the PID's lamp's bulb. Adapted from (RAE Systems, 2013)

Gas	Major Emission Wavelengths (nm)	Major Emission Lines (eV)
Ar	104.8, 106.7	11.83,
Kr	116.5, 123.6	10.64, 10.03
H_2 (deuterium)	121.6	10.2
Xe	125, 129.6, 147	9.92, 9.57, 8.44
O_2	130.2, 130.5, 130.6	9.52, 9.5, 9.49

There are 3 common lamp designs for photon excitation: D.C., A.C., and R.F. Both A.C. and D.C. (figure 1.3) designs take their name from the type of input current, though they have additional differences. D.C. excitation designs feature the electrodes embedded within the lamp directly, meaning they are in direct contact with the gas that is being excited to emit the photons. As a result, potential for corrosion of the electrodes exists, but electric noise is typically less than for other designs (RAE Systems, 2013). A.C. excitation designs feature electrodes on the outside of the lamp at high voltage and at a low radio frequency rapidly turning on and off, which helps conserve power, though there may be a longer warm up time (RAE Systems, 2013). R.F., which stands for radio frequency, is similar to the A.C. design, but with a constant frequency, typically much higher than in A.C. systems. Additionally, there is no contact at all between the excitement coils and the lamp bulb, and this means that it is necessary to tune the coil to the lamp for efficient energy transfer (RAE Systems, 2013).

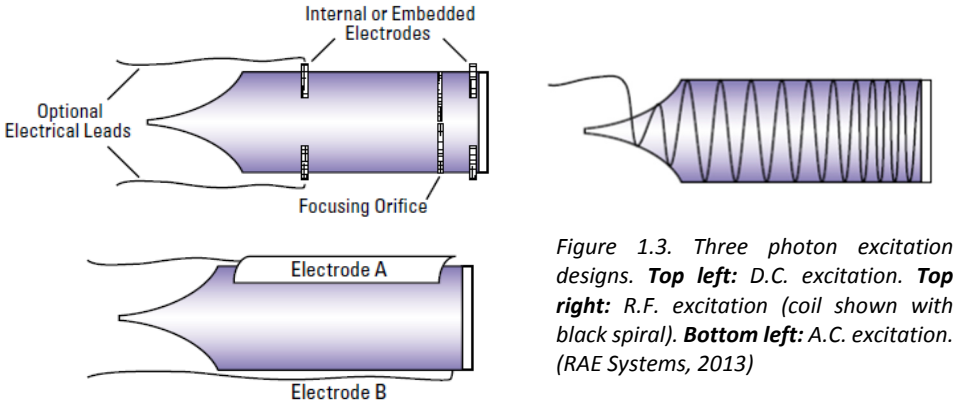

Figure 1.3. Three photon excitation designs. ***Top left:*** *D.C. excitation.* ***Top right:*** *R.F. excitation (coil shown with black spiral).* ***Bottom left:*** *A.C. excitation. (RAE Systems, 2013)*

1.3.2 Window Composition

Several materials are typically used for lamp windows as shown in table 4. This is the material which forms part of the physical lamp bulb and contains and isolates the lamp gas from the rest of the sensor and acts as an optical filter. The primary factor, which depends on both the fill gas and the window material, is the wavelength at which the sensor operates (Stober, Scolnik and Hennes, 1963). With the wavelength chosen based on the ionization energies of the VOCs of interest, window material selection is narrowed down to the materials with corresponding transparency. A material is determined to be transparent if there is no atomic absorption resonance at the wavelength of interest (Johnson, 2008). Amongst this narrowed assortment of materials, several factors, including solarization, scattering, durability, environmental tolerance, and cost must all be considered.

Solarization refers to the changes in a material's crystal structure due to UV damage (Johnson, 2008). This results in decreased transmission and consequently decreased overall sensitivity of the sensor over time, as there will be a lower net photon flux (RAE Systems, 2013). This is a primary concern as the lamp is almost exclusively irradiated by short wavelength light in the VUV spectrum.

Scattering is of greater concern for window materials that operate in the VUV spectrum, as Rayleigh scattering is proportional to $1/\lambda^4$, and thus small changes within the shorter wavelengths result in more scattering as compared to proportional changes in other spectra, such as visible light (Johnson, 2008). This results in much tighter tolerancing and quality requirements for the window manufacturing process.

Table 4. Window materials used in PID bulbs. (Johnson, 2008; RAE Systems, 2013)

Material	Wavelength of Transmission	Notes
LiF_2	105 nm	Susceptible to etching by liquid water, difficult to seal
MgF_2	115 nm	Difficult to produce, less affected by water than CaF_2
CaF_2	125 nm	Hygroscopic, high maintenance
BaF_2	135 nm	Large crystal wavelength transmittance range
Al_2O_3	142 nm	Sapphire, very expensive, very durable
SiO_2	190 nm	Fused silica, very cheap, durable.

Secondary factors, such as how the material reacts to high or low humidity, pressure, temperature, and how quickly this results in degradation all depend on the area of application and the conditions to which the sensor is subjected. Over time the window material will experience fouling, but regular cleaning (for example by using very fine aluminum oxide powder) can help alleviate this (Ion Science, 2017).

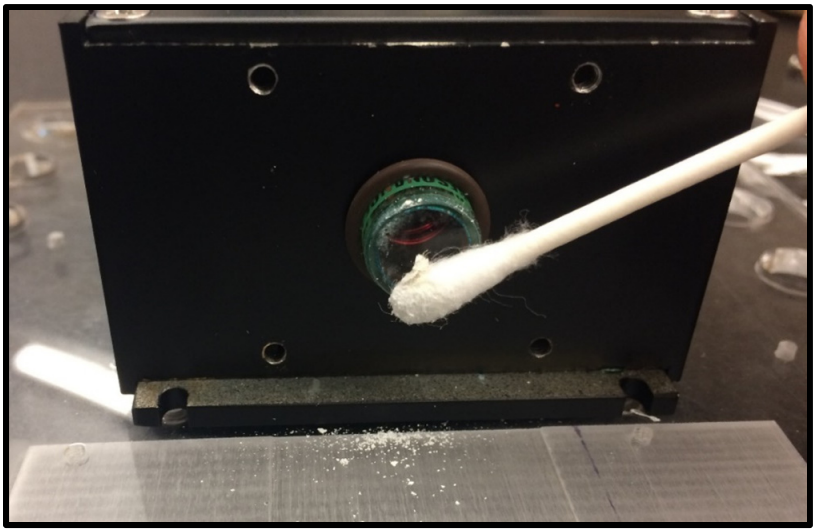

Figure 1.4. Cleaning the MgF_2 window of the lamp used in the sensor with fine aluminum oxide on a cotton swab.

1.3.3 Detector Design and General Sensor Construction

Several variations exist for the "detector" portion of the sensor, but all are based on the same general principle. Two plates are next to one another with large, opposite voltage potentials. With the purpose of the plates being to attract ions from the ionized gas sample, both increasing the surface area and the voltage differential will lead to higher sensitivity (Zhou *et al.*, 2018). Both of these factors are limited by practicality. The size of the plate and the corresponding surface area must not be too large as to make the sensor unusable in the field of application—which in the present case is on a UAV. The maximum voltage potential differential value is set by the dielectric breakdown of air. This is the point at which air is no longer an insulator and becomes electrically conductive, leading to neutralization of the voltage potential.

If the voltage is too high, above $3x10^6$ V/m (Tipler, 1987), then the plates will short circuit. However, that would require either a very high voltage (numerator) or extremely tight plates (denominator). The current is produced by the newly made ions, and then current changes can be measured, which correspond to the produced ion concentration,

which directly measures the VOCs of interest (Driscoll, 1977). The electronics behind this are discussed in chapter 3.

Sensors may either be standard rectangular plates or of another configuration. Using cylindrical plates (also known as a "long path" design) allows for a larger effective current, as this maximizes the available surface area. However, this design typically requires a higher bias voltage as the plates will be spaced further apart (RAE Systems, 2013). The rectangular plates (or "short path" design) eases the construction of proximate plates, requiring a lower voltage, but requires more sophisticated electronics as the measured current will typically be lower (RAE Systems, 2013).

After the VOCs are ionized and attracted to the plates, they form an electric current. This is then converted to a voltage, and changes in the voltage can be measured, with the voltage directly proportional to the VOC concentrations (Yamada, Hino and Ogawa, 1984). In designing the detector, the considerations involved in choosing the lamp fill gas, the window material, excitation method, and detector plate design are all addressed in chapter 3.

1.4 Issues with Established Techniques

1.4.1 Sampling Mechanisms

Currently, most air sampling is done through either aircraft flybys, satellite observations, or ground tower air monitoring. Aircraft provide the capacity for real-time, high sensitivity data, but are of relatively low temporal resolution due to the speed of collection (the airplane's speed). Additionally, aircraft field campaigns can also be prohibitively expensive. Satellites are limited to certain bandwidths and consequently only some compounds may be detected. For example, it is possible to monitor formaldehyde through satellite observation but not directly isoprene (in fact, formaldehyde measurements

are used to infer isoprene concentrations through inverse modeling, but there are many constraints in doing so) (Millet *et al.*, 2008). Air monitoring towers provide very high resolution data but it is only acquired in one spot and consequently cannot account for the heterogeneity of a typical biological system (George and Abbatt, 2010).

Currently for UAV measurements, air samples are collected in carbon filters and then transported back to a lab for TD-GC-MS analysis (Mckinney *et al.*, 2018). While TD-GC-MS is considered the standard for sample analysis, it is not a system that can be made portable very easily. As many VOCs can have extremely short lifetimes—shorter than the time between sample collection and sample analysis—they are consequently not accounted for in VOC measurements. Furthermore, the sampling technique may yield unusable data, with that only becoming apparent far afterwards, and it is not possible to adjust sampling locations based on VOC emissions.

A UAV based real-time VOC sensor is able to maintain the sampling advantages that already exist just through the use of a UAV but provides the additional accuracy of measuring short-lived VOCs due to the fast measurement and minimal sampling line length. Furthermore, with real-time analysis it is possible to act upon the data, correcting for sampling issues immediately as they become apparent (eliminating unusable flights) and being able to follow emission gradients. Nonetheless, UAVs are imperfect, being limited to sampling around 500 meters in height and around 2 km in horizontal range, and only permitting for a single point of measurement in time, issues not experienced with remote sensing methods. Furthermore, size and power restrictions make the sensing capabilities more limited than any ground or aircraft-based sensing system, and rain can damage the electronics. UAV measurements are also highly dependent on windspeed, and

the UAV's rotors may disturb the gas being sampled. Mounting the sensor below the UAV has been found to minimize potential distortions (Villa, Salimi, *et al.*, 2016). However, despite these limitations, UAVs provide an invaluable opportunity for addressing a clear gap in current measurement techniques.

1.4.2 PIDs

Commercial PIDs face around a 1 part per billion (ppb) resolution barrier which is insufficient for measurements of many biogenic VOCs. Freedman's equation suggests that this barrier may be pushed, and consequently sensitivity increased, by increasing photon flux (all other parameters held constant):

$$i = I^o F \eta \sigma \mathrm{NL[AB]}$$

Where i is the ion current generated in the PID, I^o is the photon flux, F is the Faraday constant, η is the probability that a molecule will absorb a photon to generate an excited state, σ is the probability that the excited state will successfully ionize, N is Avogadro's number, L is the path length, and [AB] is the concentration of an ionizable substance (the gas being sampled) (Freedman, 1982). A custom built PID allows for increasing sensitivity of the PID through increased photon flux, thus producing an ion current that is detectable above noise levels. Controlling parameters such as humidity and temperature is also an important issue, and perhaps can be addressed through modular design of the PID or data correction (RAE Systems, 2013). However, this is outside the scope of the present work.

1.5 The UAV

Currently, VOC measurements are recorded indirectly; gas samples are collected on the UAV and then the samples are taken offsite and analyzed using methods such as TD-GC-MS (Mckinney *et al.*, 2018). A "box" is attached to the UAV (DJI Matrice 600

Pro) containing all of the measurement components. The UAV, typically used for aerial imaging applications, is commercially available. The payload, which may be up to 6 kg, is simply attached to the bottom of the UAV, yielding a situation which allows for a "plug and play model", whereby a single UAV can easily have multiple payloads interchanged for a wide range of different measurements. Data transmission can occur through either an onboard SIM card connected to a mobile telephone carrier's network, through the UAV's shorter range (5 km) wireless controlling system that is used for flight commands, or data may simply be written onto an SD card and collected post flight.

Figure 1.5. DJI Matrice 600 Pro hexacopter UAV with no payload (photo credit: DJI).

While the UAV may carry up to 6 kg, this comes at a significant cost to battery life; increased weight means decreased flight time. The UAV, with batteries and no payload is 9.5 kg. Work by Wang (2017), demonstrated that additional onboard batteries would have a net negative effect on flight time. While the UAV would have more available power, allowing for a longer flight time, it would be heavier due to the batteries, decreasing the available flight time by an even greater magnitude. All of the payload equipment on board

is therefore powered by the UAV's batteries for maximal flight time optimization. The UAV provides a measured 5.7 amperes at 18 volts through an XT60 male outlet. All of the UAV's components, including flight rotors and payload, are powered by six TB47S batteries (each rated at 4.5 ampere hours), providing a total of 27 ampere hours at full charge, about 32 minutes of flight time. In a maximum power use scenario, the onboard sensor system would also operate at the maximum 5.7 amperes, leading to an estimated flight time reduction of around 3 minutes due to power consumed by the sensor system. A further loss of 4 minutes of flight time can be expected due to an anticipated total sensor system payload weight of 1.5 kg (assuming a linear payload weight to flight time relationship). This leads to an expected total maximal flight time of 26 minutes.

2. GLOBAL HEALTH IMPLICATIONS

2.1 An Overview of Air Pollution

The greatest environmental risk to human health in the world is air pollution (Schraufnagel *et al.*, 2019). Globally, particulate matter air pollution reduces life expectancy by approximately one year on average, with reductions of nearly two life years in polluted countries in Asia and Africa (Apte *et al.*, 2018). Besides particulate matter, other air pollutants, such as ozone, further contribute to the total mortality burden and life years lost due to air pollution (Lippmann, 1989; Anenberg *et al.*, 2010). Air pollution directly contributes to one out of every eight deaths in the world (American Thoracic Society, 2017). Globally, estimates range from 2.9 to 4.2 million premature deaths occurring annually directly due to outdoor air pollution alone (Lelieveld *et al.*, 2015; Schraufnagel *et al.*, 2019). Around 3.8 million more deaths occur annually due to indoor air pollution, and the resulting pulmonary diseases are the 4th leading cause of death globally (Ferkol and Schraufnagel, 2014; Schraufnagel *et al.*, 2019).

Most of the mortality burden is due to ozone and fine particulate matter pollution, among other compounds such as NO_2, SO_2, and CO (Folinsbee, 1992; Silva *et al.*, 2016). VOCs are directly an additional health hazard, in addition to their role in forming hazardous ozone and particulate matter pollutants (Ten Brinke *et al.*, 1998; Kim, 2011). However, the full impact of air contaminants on health is not fully understood, and many non-fatal ailments that nonetheless are major detriments to one's quality of life are due to air pollution (Folinsbee, 1992). The connection between air quality and human health is best understood based on the location or exposure source (indoor vs. outdoor), and origin (anthropogenic vs. biogenic).

Several specific common induced diseases targeting the respiratory and cardiovascular systems include chronic obstructive pulmonary disease (due to elevated ozone concentrations and particulate matter), acute lower respiratory illness (due to particulate matter), cerebrovascular disease (due to particulate matter), ischemic heart disease (due to particulate matter), lung cancer (due to particulate matter), and sick-building syndrome (due to VOCs) (Ten Brinke *et al.*, 1998; Perez-Padilla, Schilmann and Riojas-Rodriguez, 2010; Ferkol and Schraufnagel, 2014; Lelieveld *et al.*, 2015). Furthermore, air pollution is a major contributor to various heart and nervous system diseases, such as heart failure, stroke, hypertension, dementia, and other cognitive impairments (Brook, 2007; Allen *et al.*, 2014; Bos *et al.*, 2014). Better sensing and measurement systems, technical modifications to limit pollutant emission or exposure, and new and increasingly targeted treatment tools all represent necessary components to improving public health concerns regarding air and other environmental pollutants. In fact, reducing these environmental pollutants represents the primary and possibly most effective way to reduce the burden of all cancers (Danaei *et al.*, 2005). Thus, reducing air pollution is a major opportunity for improving global health and represents a significant and effective disease prevention measure (Ferkol and Schraufnagel, 2014).

2.2 Types of air pollution

2.2.1 Indoor Air

Indoor air pollution differs between urban and rural developing areas. Within rural areas of developing countries, indoor air pollution is primarily due to cooking and heating (Zhang and Smith, 2003; Perez-Padilla, Schilmann and Riojas-Rodriguez, 2010). Even though people generally spend less time indoors in developing regions (generally around 70%, compared to 90% in developed urban areas), the concentrations of pollutants are

typically much higher than in indoor urban areas (Perez-Padilla, Schilmann and Riojas-Rodriguez, 2010). Smoke toxins and particulate matter are the primary air pollutant concerns in developing rural areas (Barregard *et al.*, 2006). Because most the sources of the pollutant come from inefficient open fires (in enclosed spaces) used for cooking, women, children, and the elderly (who more often participate in household chores) are often most at risk (Zhang and Smith, 2003). The ensuing biomass burning in the cooking fires represents one of the largest sources of particulate matter (Armendáriz-arnez *et al.*, 2010). While particulate matter affects the heart and lung directly, the exact mechanism of impact is not fully understood (Schwartz *et al.*, 2005). However, the evidence for particulate matter's detrimental role to overall health is still quite explicit (Apte *et al.*, 2018).

As in developing rural areas, particulate matter pollution is a major concern in urban areas, though the sources are very different. In urban areas, particulate matter pollution indoors is often primarily due to outdoor air pollution sources, and cooking represents a smaller component source, due to more efficient cooking systems and improved ventilation (Barregard *et al.*, 2006; Leung, 2015). Frequently, outdoor sources of urban air pollution enter the indoor environment through mechanical ventilation systems positioned near ground level and through open windows and doors (Leung, 2015). The origin of particulate matter formation in outdoor urban areas is often largely due to transportation and industrial sources (Fenger, Hertel and Palmgren, 1998; Brook, 2007; Stewart *et al.*, 2017). Besides particulate matter, a major component of indoor air pollution are VOCs (Ten Brinke *et al.*, 1998; Zhang and Smith, 2003; Perez-Padilla, Schilmann and Riojas-Rodriguez, 2010). Particularly in energy efficient buildings (largely built after the

1970s) in highly developed countries, where the buildings are well insulated ("air-tight") and consequently air circulation is kept to a minimum, VOCs tend to accumulate to unsafe levels (Ten Brinke *et al.*, 1998; Zhang and Smith, 2003). Consequently, many diseases, such as sick-building syndrome, can be directly tied to VOCs (Ten Brinke *et al.*, 1998).

Health issues arising from exposure to indoor contaminants is one of the most common health concerns people face, with sick-building syndrome an increasingly common concern (Ledford and Lockey, 1994). Sick-building syndrome health aliments are typically non-fatal but can be extremely debilitating (Redlich, Sparer and Cullen, 1997). Consequently, chronic, low level indoor exposure to VOCs leads to numerous issues, with the most common symptoms including mucous-membrane irritations (eye and throat irritations, cough), neurotoxic effects (headaches, fatigue, lack of concentration), respiratory symptoms (shortness of breath, cough, wheeze), skin symptoms (rash, pruritus, dryness), chemosensory changes (enhanced or abnormal odor perception), and visual disturbances (Redlich, Sparer and Cullen, 1997).

2.2.2 Outdoor Air

Outdoor anthropogenic air pollution of particulate matter is mainly due to combustion, and thus typically tied to transportation, industry, and agricultural sources (Cohen *et al.*, 2006; Brook, 2007; Silva *et al.*, 2016; Stewart *et al.*, 2017; Zeng *et al.*, 2019). Particularly in Asia, coal burning electric power plants and intentional burning of land for agriculture produces most of the sources of particulate matter pollution (Vennemo *et al.*, 2009; Lu *et al.*, 2016; Zeng *et al.*, 2019). As a result, about 65% of the burden of disease globally due to outdoor air pollution is in Asia alone (Cohen *et al.*, 2006). As with indoor air pollution, children and the elderly are particularly sensitive (Mutius *et al.*, 1995; Sacks

et al., 2011; Simoni *et al.*, 2015). Children typically breathe more rapidly than adults, increasing their susceptibility to inhaling any air pollutants, and are also more likely to breathe through their mouths rather than their nose, significantly reducing the chance for filtration of the pollutant from the air (California OEHHA, 2003). As children's organs and bodies are still developing, there is more risk for long term damage from air pollution (California OEHHA, 2003; Sacks *et al.*, 2011).

Chronic and preexisting conditions may increase susceptibility to adverse health effects due to air pollution (Sacks *et al.*, 2011; Simoni *et al.*, 2015). As these conditions are common in the elderly, they are at increased risk of health problems due to air pollution (Simoni *et al.*, 2015). Additionally, air pollution can directly further aggravate the already existing lung, heart, and circulatory health conditions elderly populations more often face (Bateson and Schwartz, 2004; Sacks *et al.*, 2011).

There are other health concerns beside particulate matter in outdoor air pollution. Combustion of hydrocarbons, especially in the transportation sector, is a major source of NO_x (Robinson and Robbins, 1970). The high temperatures induced by combustion of fuel (especially diesel, which burns at a higher temperature than gasoline) leads to formation of NO_x from atmospheric N_2 and O_2 (Robinson and Robbins, 1970). Excessive NO_x pollution is tied to lower respiratory tract illnesses, as well as other adverse health effects, though the exact pathway is still unclear (Mutius *et al.*, 1995; Lu *et al.*, 2016). However, NO_x's biggest impact on public health comes from its chemical reaction relation to ozone—NO_x can lead to ground level ozone pollution (Zhang and Ying, 2011). Ozone, which is toxic to organic membranes, especially in the lungs, is a major ground level pollutant, especially in urban areas (Stewart *et al.*, 2017). Ozone is tied to premature aging of the lungs, decreased

lung capacity, and further cardiovascular and nervous system issues (Lippmann, 1989; Weinhold, 2008; Stewart *et al.*, 2017).

2.2.3 Other Air Pollutants

All of the previously discussed forms of air pollution have focused on low level chronic pollutant exposures. However, short-term high-level exposure is also possible and can be extremely debilitating often leading to death or irrecoverable injury, as evident by cases such as the London fog of 1952 (particulate matter). Heart attacks and sudden death are tied to short-term acute ozone exposure (Devlin *et al.*, 2012).

Additional air pollutants include biological contaminates (such as mold and bacterial spores, skin and animal dander, and organic dust), acutely toxic materials (such as lead, mercury, and asbestos), and radioactive sources, all of which may be typically experienced as chronic, low level pollutants (Redlich, Sparer and Cullen, 1997; Fenger, Hertel and Palmgren, 1998; Perez-Padilla, Schilmann and Riojas-Rodriguez, 2010; Leung, 2015).

Chronic exposure due to smaller undetected leaks by living near industrial sites is documented to increased mortality risks (Folinsbee, 1992; Bauleo *et al.*, 2019). However, more high-level exposure is possible through major leaks from chemical or biological weapons plants and various industrial accidents. For example, the leak of Bacillus anthracis spores, responsible for anthrax, in Sverdlovsk, U.S.S.R., at a weapons factory in 1979 led to 105 immediate deaths and thousands of hospitalizations (Gordin, 1997; Spencer, 2003). The industrial accident at a pesticide plant resulting in a methyl isocyanate gas leak in Bhopal, India in 1984 led to over 3800 immediate deaths and over half a million hospitalizations (Broughton, 2005). While these acute cases have very serious

consequences, most of the global burden of disease due to air pollution is ultimately due to low-level chronic exposure (Cohen *et al.*, 2006).

2.3 Pollutant Sources

2.3.1 Particulate Matter and VOCs

Particulate matter is typically classified as either primary or secondary and can be further partitioned based on the size of a particle's diameter. Most regulations begin addressing particulate matter bellow 10 micrometers in diameter size; above this threshold (roughly), particulate matter either does not exist as the large particles have trouble staying airborne and tend to settle down, or the nose and throat are able to filter the particles before they reach the lungs (Folinsbee, 1992; Jones, 2001; Brook, 2007).

Coarse particulate matter sized between 10 and 2.5 micrometers (classified as PM_{10}) represents the range at which particles enter the respiratory system, but do not enter gas-exchange regions (Lippmann, 1989; Jones, 2001; Brook, 2007). Fine particulate matter sized smaller than 2.5 micrometers in diameter (classified as $PM_{2.5}$) affects gas exchange regions (lung alveoli), and is consequently considered more harmful to health and is the basis for most particulate matter pollution regulations (Brook, 2007; Sandstrom and Forsberg, 2008; Apte *et al.*, 2018; Schraufnagel *et al.*, 2019). Ultrafine particulate matter sized under 1 micron (classified as $PM_{1.0}$) or 0.1 micrometer (classified as $PM_{0.1}$) is typically not distinguished in air pollution regulations and is poorly classified (Fenger, Hertel and Palmgren, 1998; Brook, 2007; Kumar *et al.*, 2014; Lelieveld *et al.*, 2015). Ultrafine particles, especially $PM_{0.1}$, are able to pass cell membranes and can thus be extremely toxic, being circulated through the whole body, inducing oxidative stresses, and possibly crossing the blood brain barrier (Bos *et al.*, 2014; Kumar *et al.*, 2014; Schraufnagel *et al.*, 2019). A significant toxicity component of overall air pollutant is likely

due to particles in this size range (Fenger, Hertel and Palmgren, 1998; Brook, 2007; Bos *et al.*, 2014; Kumar *et al.*, 2014).

Distinguishing aerosols and particulate matter as either primary or secondary represents the chemical source of the pollutant. Primary particles are generally larger than secondary particles (Fenger, Hertel and Palmgren, 1998). Both primary and secondary pollutants may have both biogenic and anthropogenic sources (Phalen, 2004). In terms of human health impact, the actual source should have little impact on the toxicity of particulate matter; the particulate matter itself is harmful, regardless of its origin (Fenger, Hertel and Palmgren, 1998; Phalen, 2004). Most observed differences are likely due to other pollutants associated with the particulate matter, such as ultra-fine particles, VOCs, or compounds such as SO_2 which accompany the particulate matter being measured (Folinsbee, 1992; Fenger, Hertel and Palmgren, 1998; Phalen, 2004; Kumar *et al.*, 2014).

Aerosols or particulate matter are directly released through forest fires (soot) and volcanic activity, through dust picked up by the wind and salt (ocean spray), as well as through anthropogenic activities associated with combustion (Fenger, Hertel and Palmgren, 1998; Sandstrom and Forsberg, 2008; Anenberg *et al.*, 2010; Stewart *et al.*, 2017). Dust and sea salt primary sources of are by far the largest contributors to total particulate matter air pollution globally (Brook, 2007; Lelieveld *et al.*, 2015; Stewart *et al.*, 2017). Consequently, areas such as Spain, and even regions as far away as the Caribbean, may experience high seasonal particulate matter pollution due to dust picked up and carried from the Sahara-Sehal desert (Sandstrom and Forsberg, 2008). Desert dust may also be a large source of biological air pollution, by carrying various bacteria and fungi (Sandstrom and Forsberg, 2008). Besides these large sources of primary particulate matter and aerosol

pollution, secondary aerosols may form through oxidation of biogenically and anthropogenically emitted VOCs in the air.

Autooxidation of VOCs forms nearly half of secondary organic aerosols indoors, and VOCs are a major source of particulate matter pollution outdoors (Fenger, Hertel and Palmgren, 1998; Pagonis *et al.*, 2019). Within urban areas, emitted VOCs are typically from transportation, industry, and increasingly, consumer products (Fenger, Hertel and Palmgren, 1998; McDonald *et al.*, 2018). Consumer products, such as different cosmetics, paints, cooking, and building materials, have increasingly become the dominant source of VOCs, and thus may represent a new sector that may need further regulations to achieve further reductions in air pollution (Leung, 2015; McDonald *et al.*, 2018). Furthermore, VOCs emitted by consumer products are typically more reactive than those emitted industrially or by automobiles, leading to a larger contribution to secondary organic aerosols formed (McDonald *et al.*, 2018). A larger component of the public health burden of disease due to air pollution is consequently becoming decentralized, which will complicate effective regulatory measures.

2.3.2 Ozone

Ozone's detrimental role to health was noticed in the 1960s, when observations were made demonstrating that athletic ability (running) of students decreased when high levels of ozone were present (Folinsbee, 1992). An athlete running a marathon using 70% of their maximal lung air capacity consumes about as much air as a sedentary person does over the course of two days, making athletes a particularly vulnerable population, reducing performance and causing conditions such as asthma (Bos *et al.*, 2014; Schraufnagel *et al.*, 2019). Tropospheric ozone is usually formed by oxidation of CO and various VOCs by the

OH radical in the presence of NO_x (Jacob, 1999). Ozone occurrence is due to ozone production through a series of chemical reactions in the atmosphere, with precursors typically due to transportation emissions and various VOC emissions—leading to elevated ozone levels in urban areas, as well as direct ozone emissions from photocopiers during printing (Tuomi *et al.*, 2000; Mauzerall *et al.*, 2005).

2.4 Legal Standards and Policy Protections

Controls over air pollution date back to the Napoleonic era, when rules over various odors and smells were established in Paris (Fenger, Hertel and Palmgren, 1998). Historically, only after major environmental pollutant episodes with significant human health damages are concerns raised by local people and consequent legal protections established (Zeng *et al.*, 2019). The most major influential event was the London fog of December 1952, where over the course of 4 days over 4000 people died directly (immediately) due to inhalation of extreme air pollution from particular matter, smoke, and sulfur dioxide (Logan, 1953; Wilkins, 1954; Ito *et al.*, 1992). This quickly led to the British Clean Air Act of 1956, which limited use of coal for home heating and marked a turning point in urban air pollution (Fenger, Hertel and Palmgren, 1998). Similar famous recorded incidents occurred beforehand in Belgium and Pennsylvania (Wilkins, 1954). These acute incidents are surpassed in public health impact only by major outbreaks such as the cholera epidemic of 1854 and of the influenza epidemic of 1918 and 1919 (Logan, 1953). The immediate death tolls do not include the thousands of individuals whose decreased lifetimes were only evident decades later (Ito *et al.*, 1992). In the United States, the Clean Air Acts of 1963 and 1970 and their further amendments and modifications provide the basis for air pollution protections and represent the point of recognition and acceptance of

the hazards of air pollution in the United States (Folinsbee, 1992). Laws established with similar motivations to the U.S. and U.K. Clean Air Acts exist in nearly all countries (Fenger, Hertel and Palmgren, 1998). As an example, China experiences some of the world's worst air pollution (Vennemo *et al.*, 2009). However, new laws are constantly established to ensure that air pollution levels are lowered (Zeng *et al.*, 2019). Sustained reductions in air pollution exposure through decreased emissions increases life expectancy, a clear and measurable policy goal (Arden Pope III, Ezzati and Dockery, 2009).

Part of the difficulty with implementing increasingly strict air pollution regulations is the determination of what air pollution is and justifying thresholds set by regulators. Broadly speaking, air pollution is defined as "any substance which may harm humans, animals, vegetation or material" (Kampa and Castanas, 2008). However, any substance can potentially be harmful, and furthermore there is no such thing as a safe level or threshold of pollution (Brook, 2007; American Thoracic Society, 2017; Schraufnagel *et al.*, 2019). Breathing in less particulate matter is always better for health than breathing in more, and clearly anthropogenic sources which adversely affect health should be controlled in some way as to limit their impacts (Brook, 2007). Yet a blanket rule of an amount X being the acceptable threshold is often quite arbitrary (Fenger, Hertel and Palmgren, 1998). Many locations across the U.S. and world may "naturally" exceed U.S. EPA or other regulations, and regulating naturally occurring "pollution" is not particularly useful in most cases (completely clean air is not found in nature) (Anenberg *et al.*, 2010). An exception may be wildfires, where human fire policies and practices play a role in the "naturally" occurring fires (or the lack thereof). There may be biogenic emission differences in wildfires occurring after years of suppression (a human intervention) as compared to wildfires

occurring at more natural intervals (Wiedinmyer and Hurteau, 2010; Granier *et al.*, 2011). Generally, however, regulations regarding air pollution can only target anthropogenic emissions, and consequently regulations must take into account natural biogenic variations (Weinhold, 2008).

2.5 Further Health Impacts

Besides direct health implications, pollutants play a large role in agriculture production (Vennemo *et al.*, 2009; Zeng *et al.*, 2019). Excessive smog, particularly in India, China, and parts of southeast Asia, can significantly lower crop yields (in parts India, crop yields have fallen by 50% due to excessive particulate matter and ozone) (Burney and Ramanathan, 2014). While various pollutants affect precipitation, temperatures, and climate more broadly, particulate matter and ozone pollutants are directly tied to plant toxicity and are directly responsible for most of the yield losses (Chameides *et al.*, 1999; Burney and Ramanathan, 2014). This has major implications for food security and nutrition, providing a further channel for air pollution to adversely affect human health (Chameides *et al.*, 1999; Burney and Ramanathan, 2014). As pollutants affect humans and plant life, they likewise affect domestic and wild animals (Catcott, 1961; Lilllie, 1972; Cox *et al.*, 2017). Animals may themselves experience health issues due to decreases in plant life and consequent food supply, besides the direct impact on their health from air pollution inhalation (Catcott, 1961; Lilllie, 1972). Communities dependent on animal food sources for sustenance may also experience increased risk of food insecurity and malnutrition due to animal losses from air pollution (Lilllie, 1972; Cox *et al.*, 2017). In addition to direct food concerns and consequences, economic costs naturally arise as well from the lost animal and agricultural yields (Catcott, 1961; Chameides *et al.*, 1999; Cox *et al.*, 2017).

As a result, human health may be further harmed if economic resources must be diverted away from healthcare to address food issues.

Additional impacts on health can come from the degradation of materials in the face of high levels of pollutants like ozone (Lee, Holland and Falla, 1996). For example, rubber car tires prematurely degrade in the presence of ozone, increasing risk for automobile accidents, an additional indirect adverse impact on human health due to air pollution (Lee, Holland and Falla, 1996).

2.6 Policy Considerations, Challenges, and Regulation Opportunities

In the United States, a decrease of 10 micrograms per cubic meter in the concentration of fine particulate matter ($PM_{2.5}$) is associated with an average life expectancy increase of 0.61 years (over 7 months) (Arden Pope III, Ezzati and Dockery, 2009). Consequently, reductions in air pollution can account for up to a 15% overall increase in life expectancy (Arden Pope III, Ezzati and Dockery, 2009). This direct link between life expectancy and particulate matter pollution, which is easily measured, provides obvious justification and motivation for regulations to limit and decrease emissions of particulate matter.

Full understanding of pollutant sources and chemistry is crucial for establishing air pollution standards, as effective reduction protocols cannot be implemented without specific targets (i.e., deciding who will reduce what, by how much, and in what way) (Fenger, Hertel and Palmgren, 1998). With air pollution a major hazard for global health, it is clear strong regulations must be in place. Air pollution knowns no borders, and thus a global response is necessary (Zhang and Smith, 2003; Cohen *et al.*, 2006; Lu *et al.*, 2016). This is possible through international agreements, such as the Montreal Protocol which

limited the use of chlorofluorocarbons (CFCs) quickly and effectively (Jacob, 1999; DeSombre, 2000; Molina *et al.*, 2009). The Montreal Protocol was successful as industry alternatives could be created to CFCs, emission sources were limited and could be directly targeted, and clear science existed demonstrating the link of CFCs to stratospheric ozone degradation and the corresponding serious environmental and health implications (Fenger, Hertel and Palmgren, 1998; DeSombre, 2000; Molina *et al.*, 2009; McDonald *et al.*, 2018). CFCs are only produced synthetically, and thus the "safe" or "natural" level is zero (DeSombre, 2000). The ensuing stratospheric ozone degradation has nonetheless caused serious health issues, particularly regarding skin cancers and suppressed immune systems in certain regions due to increased UV-B radiation exposure (Leaf, 1993; Gruijl and Leun, 2000). However, the ozone recovery process is now ongoing due to the implemented regulations (DeSombre, 2000; Molina *et al.*, 2009).

Since VOCs, particulate matter and aerosols, ozone, and many other potential pollutants are naturally occurring in various concentrations (though perhaps above preindustrial concentrations) at different times in different places, a response as unified as was for CFCs is unlikely to be as straightforward (Lee, Holland and Falla, 1996; Fenger, Hertel and Palmgren, 1998; Cohen *et al.*, 2006; Weinhold, 2008; Molina *et al.*, 2009). Public health forms a strong moral foundation for any action; it could be argued that if a particular emission has no negative health consequences, then little legal basis or motivation exists for limiting it (Redlich, Sparer and Cullen, 1997; Fenger, Hertel and Palmgren, 1998; DeSombre, 2000; Mauzerall *et al.*, 2005). Yet the health implications of VOCs, particulate matter, ozone, and related pollutants are clear and consequential (Zhang and Smith, 2003; Cohen *et al.*, 2006; Allen *et al.*, 2014). Limiting natural sources of

biogenic emissions is meaningless; even if air quality is as poor as it was in London in the winter of 1952 with deaths occurring on the spot, but the source of the air pollution is a nearby volcano eruption or dust storm irrespective of human activity, then typically nothing can effectively be done to limit emissions (Ledford and Lockey, 1994). Limiting human settlement zones away from high altitude areas, forested areas, dusty areas, or other high-risk localities is not practical either. Thus, the focus of regulations must be on direct anthropogenic emission sources as well as on anthropogenic activities which change biogenic emission sources (DeSombre, 2000; Mauzerall *et al.*, 2005; Molina *et al.*, 2009). If anthropogenic activity changes fire patterns such that there is a net increase in emitted pollutants, then certainly emissions, despite being from a biogenic source, can be addressed (Wiedinmyer and Hurteau, 2010; Granier *et al.*, 2011).

A difficult moral decision arises regarding the purpose of air pollution regulation. In the case that public health is the primary consideration or motivation, then regulations must be unequally implemented due to biotic variations (Molina *et al.*, 2009). Fairness arguments can go one of two ways. Either it is unfair that different countries (or even regions within a single country) have different health outcomes, or it is unfair that different countries have varying levels of permissible air pollutant emissions. Though this is an unsettled debate, U.S. regulations typically address overall permissible pollution levels, taking into account both biogenic and anthropogenic emissions (with possible exceptions based on extenuating circumstances such as natural disasters) (Fenger, Hertel and Palmgren, 1998; United States EPA, 2019).

In order to improve global health and increase life expectancy, several actions regarding air pollutants must be made. The highest priority concern is decreasing emissions

of long-lasting pollutants, which hold potential for further climate change mechanisms and stratospheric ozone degradation (Molina *et al.*, 2009). With particulate matter correlated as perhaps the most significant human health concern, determination of the exact mechanism of human injury is necessary, as well as further insight into ultra-fine particulate matter (PM_1 and $PM_{0.1}$) (Phalen, 2004; Schwartz *et al.*, 2005; Brook, 2007; Arden Pope III, Ezzati and Dockery, 2009; Anenberg *et al.*, 2010; Kumar *et al.*, 2014; Schraufnagel *et al.*, 2019). More motivation and a stronger basis for particulate matter pollution control can be established through linking certain biogenic emissions to anthropogenic actions in addition to anthropogenic emissions. Improvements to VOC emission and sink inventories in indoor and outdoor urban environments, as well as biogenic VOC emission sources, along with sources of pollutants such NO_x, will provide a firmer foundation in understanding pollutant chemistry (Brook, 2007; Anenberg *et al.*, 2010; Zeng *et al.*, 2019). Economic incentives structed on a framework such as the Montreal protocol with clear improvements in global health can address the massive global health burden of air pollution (DeSombre, 2000; Mauzerall *et al.*, 2005; Cohen *et al.*, 2006; Molina *et al.*, 2009; Vennemo *et al.*, 2009; Apte *et al.*, 2018).

3. DESIGN PROCESS

3.1 Design Criteria

In order to develop a UAV based sensor system capable of measuring biogenic VOCs, several specific design goals were determined. The instrument must be sensitive to at least 1 ppb (the current limit of commercially available PIDs), response time must be near real-time (the major inadequacy of current UAV sampling techniques), and the sensor system must be mountable on a UAV (if the system is not easily portable, it will not useful). This prioritization process is demonstrated through the quality function deployment analysis (house of quality diagram) in table 5. Additional sensor criteria and features, such as humidity and temperature control, VOC selectivity, and wireless data transmission, while beneficial and immensely important to improving sensing capabilities, were ultimately deemed secondary priorities to establishing the necessary sensitivity and time response attributes and meeting the physical restrictions necessary for the UAV based measurements and are thus beyond the scope of the present work. The custom-built sensor system is necessitated by the lack of commercially available PIDs meeting the necessary specifications, likely due to the limited market which is primarily targeted at indoor air quality monitoring, with measurement requirements typically in the parts per million (ppm) range.

Table 5. Design criteria prioritization through quality function deployment analysis (house of quality diagram).

Design Choices / Sensor Requirements	**Importance**	Lamp with large photon flux (10^{15})	Minimal dead volume in ionization chamber	Maximal total current used 5.7 amperes	Pressure and flow control	Narrow plate distance	All sensor components attached to single base	No off-gassing materials	Humidity and temperature control	Large detector plate surface area	**Total**
Minimum 1 ppb VOC Sensitivity	5	H	M			H		H	M	H	210
Accurate Measurements	4	H	M		H	H		H	H	H	228
Response Time under 1 minute	4	H	H		L	H				H	148
Sensor Fully Powered by UAV	3	M		H	L		L		L		45
Total Sensor Weight Below 5.5 kg	2	M	M	H		L	L	L			36
Sensor Easily Mountable and Rugged	2	M				L	H	L		L	30
Total		138	69	45	43	121	23	85	54	119	697
Relative Weight (Priority)		19.80%	9.90%	6.46%	6.17%	17.36%	3.30%	12.20%	7.75%	17.07%	

3.2 CAD Model

Solidworks 2019 was used for CAD modeling of the sensor. Several views of the initial model are shown below. The laser cut components of the support material of the sensor were taken directly from the model.

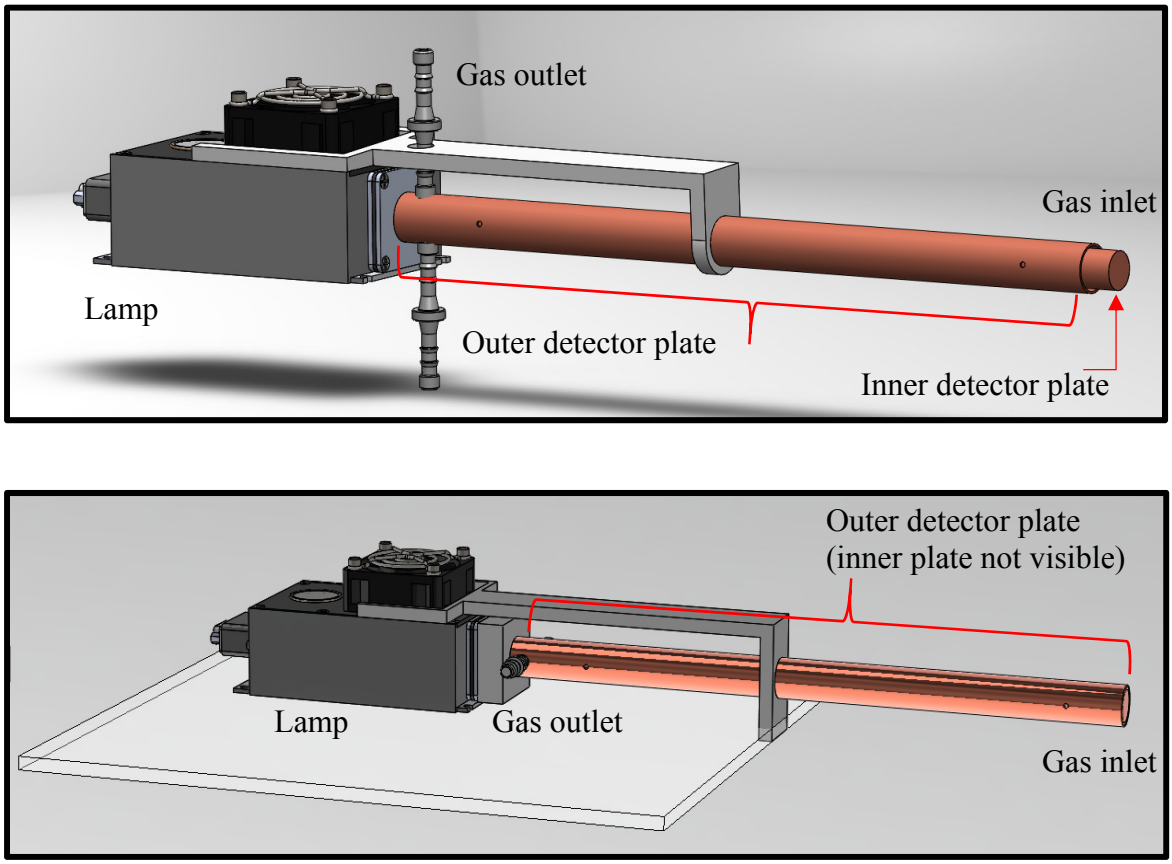

Figure 3.1. Development of the Solidworks model of the sensor featuring design iteration 1 plates. For scale, the copper detector plates are approximately 30 cm long, and the lamp enclosure about 22 cm long. ***Top:*** *Initial sensor design.* ***Middle:*** *Iteration 1 plates of the sensor on the acrylic mounting plate.* ***Bottom:*** *The PID lamp used in all designs (lamp design credit: Resonance Systems).*

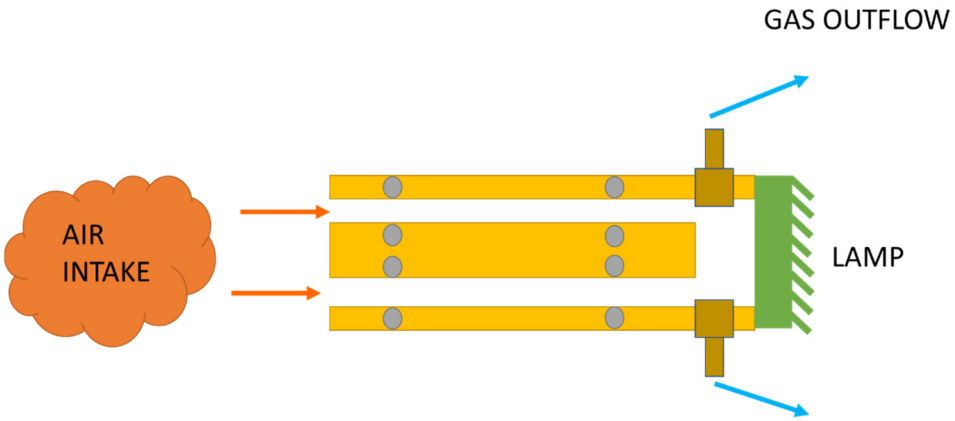

Figure 3.2 Pictorial cross section representation of the iteration 1 plate design. The detector plates are shown in yellow (with the tempered glass dowel pins in gray). The copper rod detector plate is the inner component, and the pipe forming the outer detector plate is the two outer components.

3.3 Construction

Air flow through the system is show in the schematic in figure 3.3 below. Three different plate detector designs (which form the ionization chamber) were ultimately produced, with some minor changes in support material between iterations. Electronic component design, including the lamp, was constant between sensor iterations.

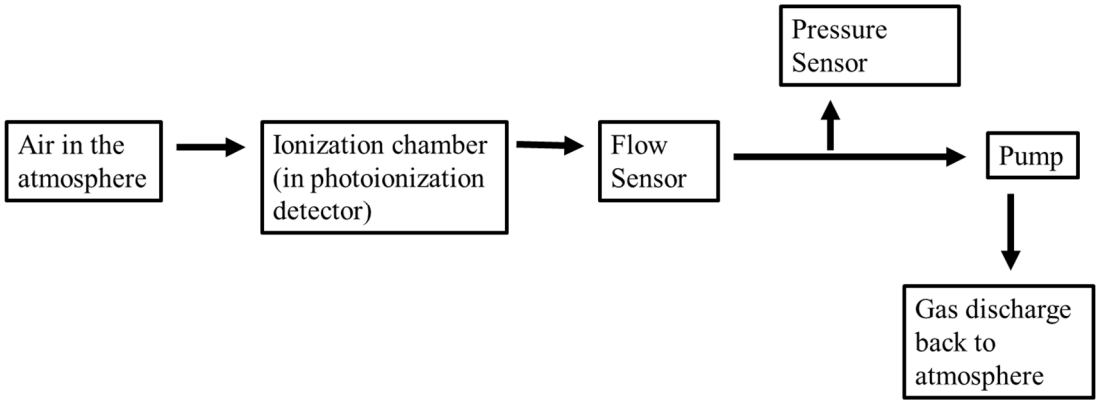

Figure 3.3. Schematic demonstrating flow of gas through the system. Air generally flows from one unit to the next, though the pressure sensor has a common inflow/outflow, similar to a gauge, and is thus shown as a side branch. All measurements take place before the pump to avoid possible leaks.

3.3.1 Inlet and Detector Plates

3.3.1.1 Plate Design Iteration 1

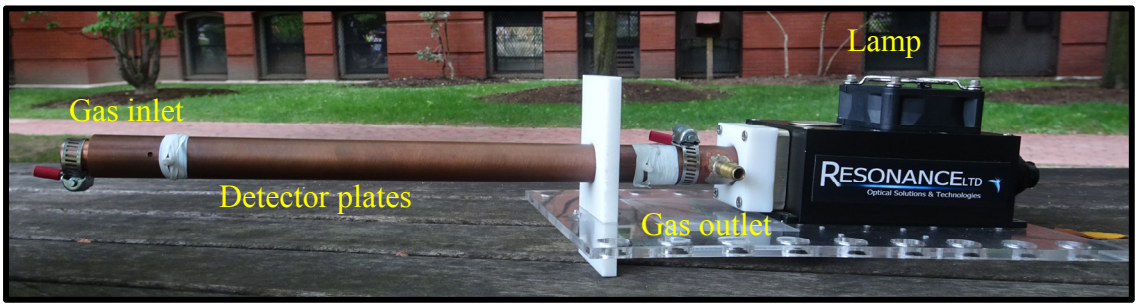

Figure 3.4. The complete sensor with the iteration 1 plates. For scale, the entire sensor from tip to tip is about 55 cm long. Moving from left to right, the red tip is the insulation on the ring terminal, attached with the gray pipe clamp to the inner copper rod. The white stripe is PTFE sealant tape and an aluminum oxide rod. The white upright component is the PTFE support bar, followed by an additional PTFE sealant stripe, a ring terminal, and one of the two brass gas uptake adapters. The system is then fit into a PTFE fitting screwed onto the lamp (the black box with the "Resonance" logo). The entire sensor was then mounted on the clear acrylic laser cut base.

101 copper (also known as "superconductive", or "low oxygen") was used for both the rod and the pipe for optimal electron transmission. The space separating the rod and the pipe allows for gas to brought into the system. The pipe's dimensions and tolerancing were appropriate when received directly from the manufacturer (McMaster-Carr). Three sets of holes were drilled into the pipe (outer plate): one 6.35 mm (0.25 in.) hole at 19.05 mm (0.75 in.) from the end through the pipe for the gas uptake adapters, and two 1.99 mm (0.0785 in., size 47 drill bit) holes for the tempered glass (Pyrex brand) separating dowel rods (shown in gray in figure 3.2). Likewise, the rod (inner plate) had two 1.99 mm (0.0785 in.) holes drilled, aligned with the ones in the outer plate. It was necessary to turn and polish the rod down to 13.84 mm (0.545 in.) diameter in order for the rod to fit well within the outer plate while remaining electrically isolated. A super fine surface finish was achieved using P400 grit sandpaper, follow by a finish pass using a Scotch-Brite sponge pad, though the exact surface finish at this scale has little influence on the effective electric field. Temporary PTFE (Teflon) bushings were created using a lathe in order to properly space the plates during the drilling process on the mill.

However, as the holes for the tempered glass were particularly small, the drilling process was especially difficult. Furthermore, upon assembly, the tempered glass repeatedly shattered. It was then replaced with a ceramic material—aluminum oxide, also an electric insulator. 5 rods, 3 mm in diameter and 32 mm long, were donated by Cemanco Corporation, and the existing holes in the copper were slightly enlarged. The holes were then sealed using PTFE sealant tape (Teflon tape). While ultimately a successful assembly, 2 rods shattered during the assembly process, demonstrating the unsuitability of the existing design for field testing (which is addressed in the following design iterations).

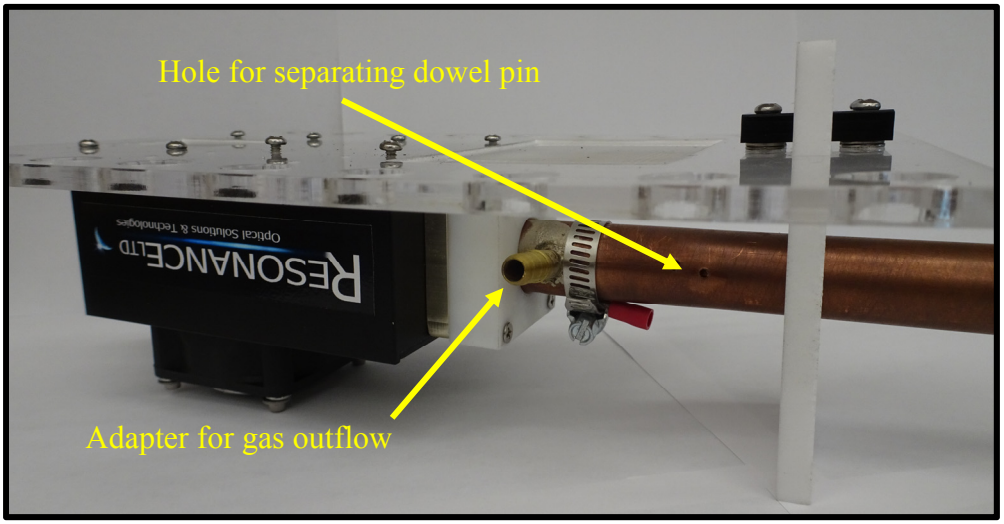

Figure 3.5. A close-up view of the sensor with plate design iteration 1. The silver around the brass gas uptake adapter is excess silver solder from the brazing process. The PTFE sealant and aluminum oxide rod are removed here, revealing the underlying hole.

The brass gas uptake adapters were brazed using silver onto the pipe, with preparation using Harris Stay-Silv white brazing flux, and following brazing quenched in cold water. The pipe and adapters were then polished to remove oxidation induced during the brazing process. Due to the size of the copper pieces, brazing was non-trivial as the rod tended to radiate as much heat as the standard torch (natural gas burning) imparted, requiring the use of two torches. Thus, in order to ease the electronic soldering process, all

the electronics were soldered onto ring terminals that were then mechanically attached to the rod and pipe using pipe clamps.

3.3.1.2 Plate Design Iteration 2

Figure 3.6. The complete plate design iteration 2 sensor as used in testing. The bottom is sealed with a PTFE bushing, one brass adapter is used as a gas inlet, the other as an outlet.

Following successful completion of the initial sensor testing phase with the first iteration sensor design, several changes were instituted. The long "Pinocchio nose" design and spaced gas inlet/outlet design was replaced by a shorter model. This immediately cut over half the weight and simplified laboratory testing to ensure a more universal gas inlet system was used, minimizing potential leaks.

The system was equipped with gas inlet and gas outlet brass gas uptake adaptors, one for each flow direction. The end of the chamber, which would have previously functioned as the gas inlet, was sealed using PTFE in a sort of "bushing shape" force fit. Besides acting as a seal, this also provided increased structural support, allowing for removal of one of the aluminum oxide ceramic dowel pins, greatly increasing the ease of system assembly and more generally improving sensor robustness.

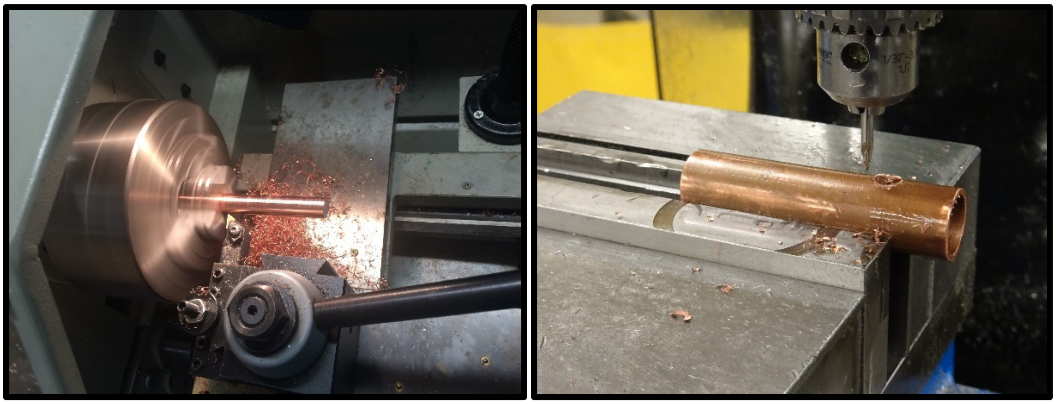

Figure 3.7. ***Left:*** *turning down the inner copper rod to the appropriate diameter on a lathe.* ***Right****: Drilling a pilot hole in the outer copper pipe on a mill.*

By turning down the side of the rod closest to the lamp (opposite the PTFE bushing) and creating a PTFE "bumper rod", the robustness of the system was increased—a crucial quality for a UAV-based sensor. While the previous plate design was relatively fragile and insecure (leading to unstable voltage isolation and frequent structural component damage), the bumper rod provided a guarantee of electrical isolation by allowing the PTFE to hit the inner wall of the copper pipe before the copper rod did, in case any component unintentionally shifted. Furthermore, construction was much simpler due to the smaller size and new mounting mechanism.

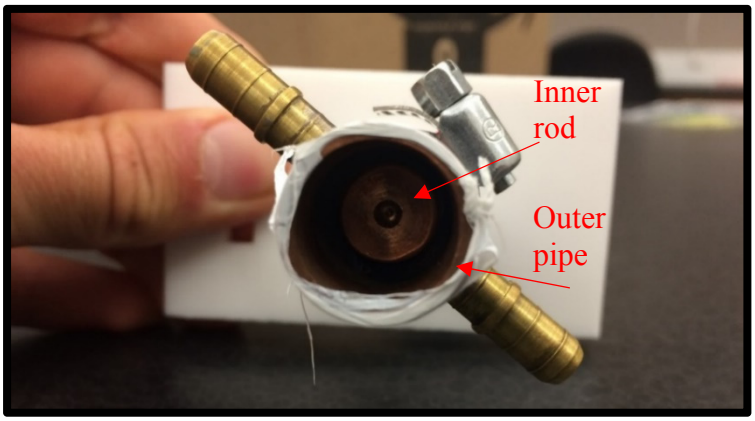

Figure 3.8. The view from the side of the lamp inside the gas chamber of the plate design iteration 2 sensor; the diameter of the inner rod appears narrower than in reality—only the tip was so narrow. The indentation in the center of the rod is from the machining process and does not affect functionality. The PTFE sealant tape along the edge was used to ensure a leak-free force fit with the PTFE mounting block.

3.3.1.3 Plate Design Iteration 3

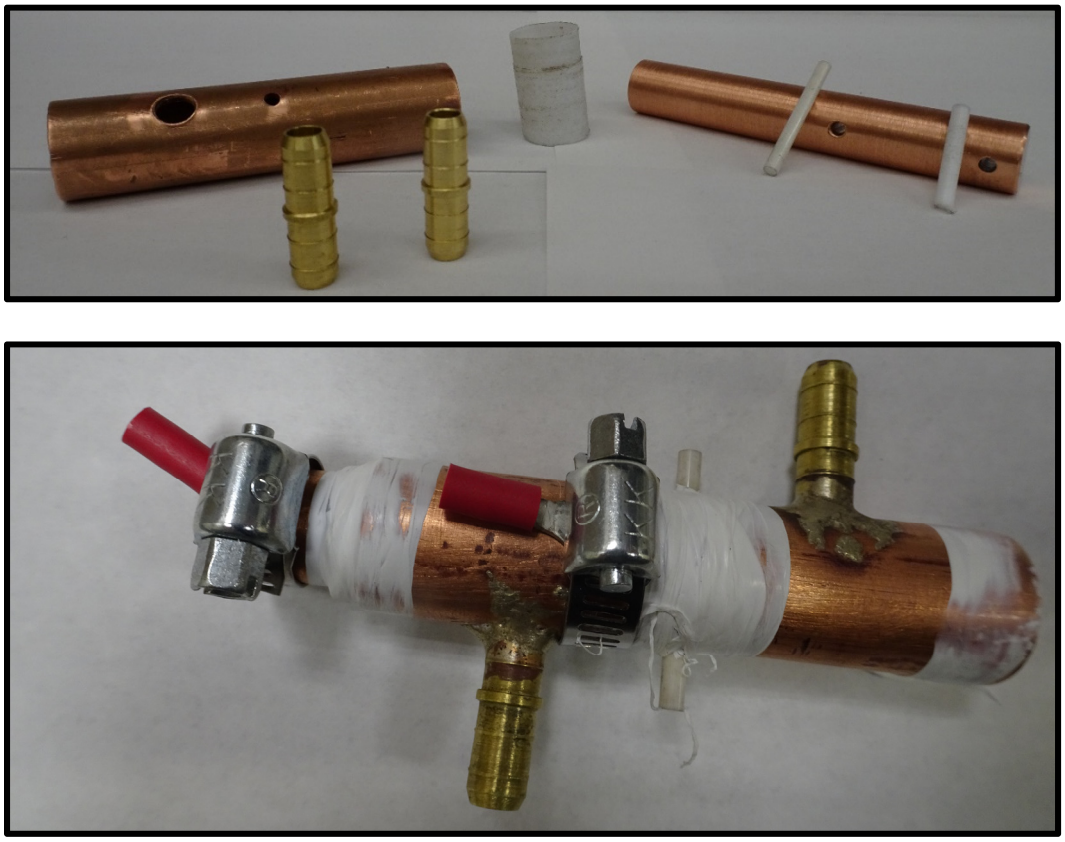

Figure 3.9. ***Top:*** *The components of the iteration 3 plate design before assembly or brazing. The longer white rod is aluminum oxide, the shorter one PTFE.* ***Bottom:*** *The complete iteration 3 plate design sensor as used in testing. The sensor includes all the components shown in the top image, as well as pipe clamps, ring terminals, and PTFE tape used as a sealant.*

After successful laboratory testing of the second plate design iteration, several changes were made to decrease the volume of the sensor and ensure better circulation of the sample gas. Both plates were limited to a length of 7.62 cm (3 in.). The outer pipe features one brass gas uptake adaptor at 1.905 cm (0.75 in.) from the end, and the second adaptor on the opposite end rotated 180˚, brazed using the same procedure as on the previous plate design iterations. One 3 mm hole was drilled in the center (3.81 cm (1.5 in.) from the either end) of the outer pipe (and through the inner rod) for the aluminum oxide pin. This was then sealed with PTFE sealant tape. The outermost part of the copper plates was sealed as before using PTFE in a sort of "bushing shape", extending 1.27 cm (0.5 in.)

in-between the copper plates, making the effective length of the sensor 4.445 cm (1.75 in.) The internal copper rod was uniformly 1.384 cm (0.545 in.) in diameter.

Figure 3.10. ***Left****: brazing the first of two brass inlet pipes onto the outer copper rod.* ***Right:*** *quenching the successfully brazed piece in cold water; notice the dramatic oxidation of the copper—this is removed during assembly.*

3.3.2 Supporting Material

In order to ensure that even trace VOC off-gassing would not occur, all structural parts of the system that were in direct contact with the copper plates were one of metal, ceramic, or PTFE (as all other plastics would interfere with accurate VOC measurements). A PTFE support piece was milled to slide onto the outer copper pipe such that it could be secured onto the acrylic base plate (which would later be mounted on the UAV). The copper pipe was additionally supported through a PTFE block mounted directly onto the lamp around the emission window. As PTFE is very soft, threading the copper pipe onto it was impossible and instead a force fit was used. The block was mounted onto extended screws that also held the metal block which enclosed the lamp's PID bulb.

The base plate was laser cut from acrylic with circular slots around the plate perimeter to provide a single adaptable mounting mechanism for the complete system. The lamp was then screwed onto the underside of the plate, and a small acrylic piece screwed into the top of the plate, securing the copper pipe supporting PTFE piece. Indentations were

rastered on the top of the plate to secure and organize the voltage regulator plates, the pump, and the Raspberry Pi (discussed below in section 3.2.3).

In order to connect the pump, which determines flow direction and pulls the gas through the system, with the copper components, PTFE tubing was used, which is one of the few tubing materials that will not interfere with VOC measurements (Place *et al.*, 2009). It was especially important to avoid the more commonly used Tygon tubing, which while considered chemically stable, tends to both emit and absorb VOCs (Place *et al.*, 2009).

3.2.3 Electronic Components

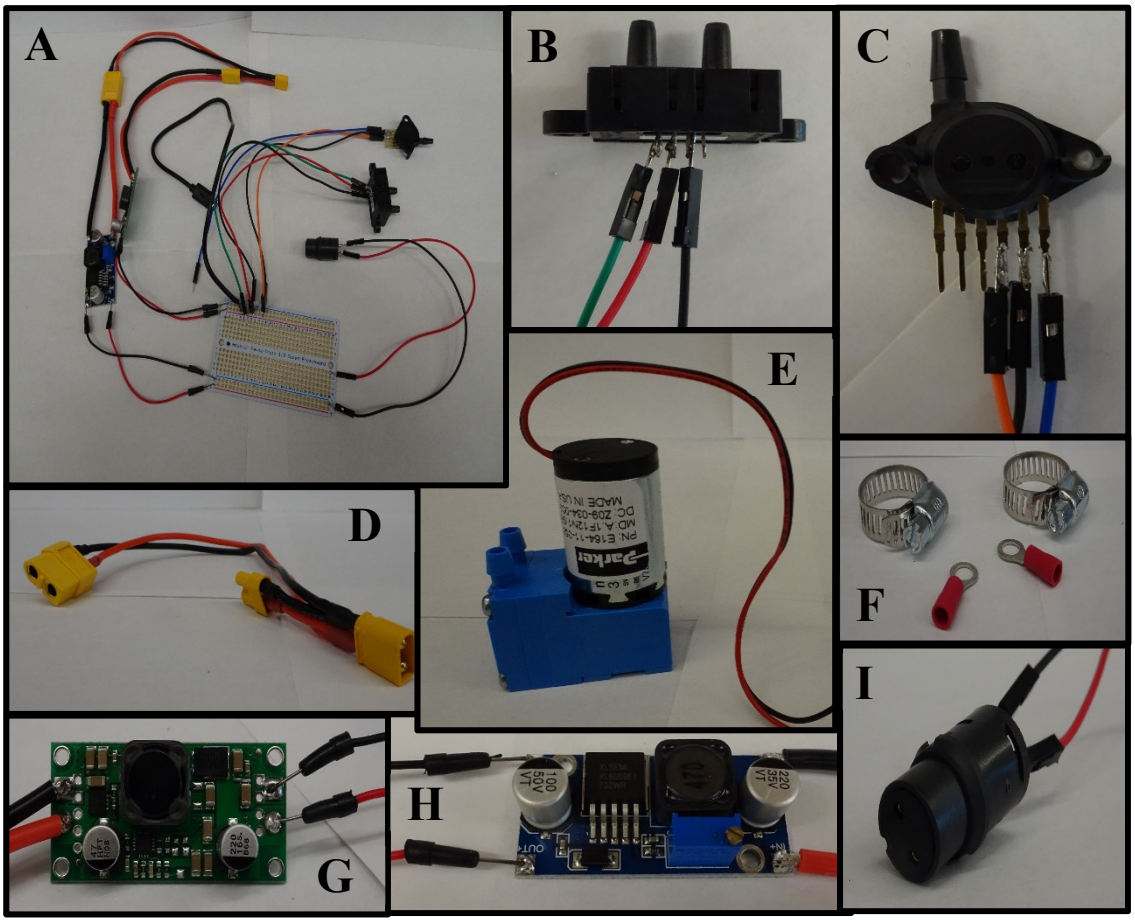

Figure 3.11. Electric components used. ***A****: The two electric branches on the bread board, 24 volts on the bottom, 5 volts on top.* ***B****: The Honeywell airflow sensor (HAFBLF0750CAAX5).* ***C****: The NXP air pressure sensor (MPX4100A).* ***D****: The XT60 and XT30 UAV connection cables.* ***E****: The Parker CTS 5-volt pump (E164-11-050).* ***F****: The two pipe clamps and ring terminal which are mechanically mounted on the detector plates (not shown).* ***G****: The Pololu 5V step-up/step-down voltage regulator (S18V20F5).* ***H****: The 4A step-up DC-DC converter (XL6009).* ***I****: The PID lamp power adapter (EN3).*

The UAV features an XT60 male cable for the electric outlet. A female connection splitting the power into two XT30 connections allowed for effective voltage control. One connection went to a Pololu 5V step-up/step-down voltage regulator (S18V20F5), which converted the UAV's 18 volts to 5 volts at 2 amperes, providing one electric branch. The second connection went to a XL6009 step-up voltage regulator which converted the UAV's 18 volts to 24 volts at 4 amperes. This then formed the second branch, which itself

separated into two components—one going straight to the lamp, the other to the copper plates.

With a potential of 24 volts across the detector plates, electrons freed during the ionization process form a current. This current is then fed into either an electrometer for direct testing or to the transimpedance amplifier (TIA). The TIA can take current of up 100 nanoamperes, but this can easily be adjusted be swapping the TIA's internal resistors. The current signal is both converted to voltage and amplified.

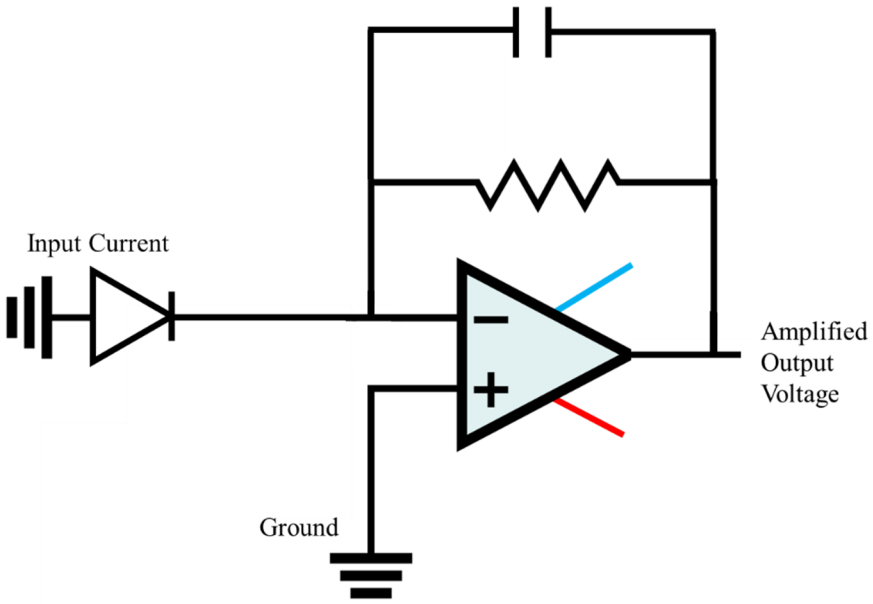

Figure 3.12. A simplified general TIA schematic; input current is amplified and converted to voltage. The TIA used was built by Jim MacArthur of the Harvard Physics Electronics Shop. The internal voltage of 9 volts (blue and red cables) is given through two 9-volt batteries.

A Parker coreless CTS micro diaphragm pump (E164-11-050), operating at 5 volts and at 0.11 amperes was used. The PTFE tubing connected the brass outlet to the pump, and the pump can discharge the sample to the atmosphere from the rear of the UAV away from the gas intake. The pump was directly connected to a 5-volt input power source from the breadboard. Though the pump is rated to operate between a 1.2 and 2.5 liters per minute flow rate (figure 3.14), only a 1.5 liter per minute flow rate was observed.

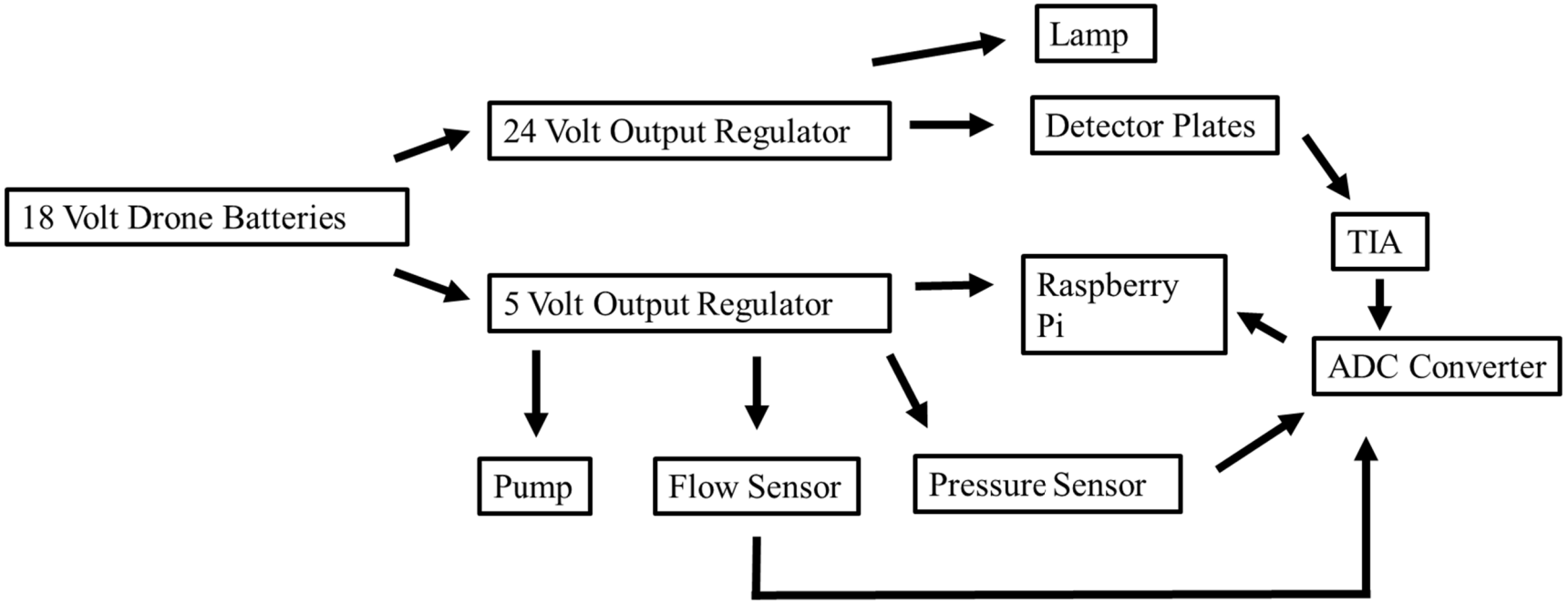

Figure 3.13. Schematic demonstrating electric pathways. Power goes to the lamp and pump, where no output signal is given. The pressure and flow sensor are analog and must pass through the ADC before giving digital output to the Raspberry Pi. The generated current from the detector plates is amplified and converted to voltage in the TIA before going to the ADC and then to the Raspberry Pi.

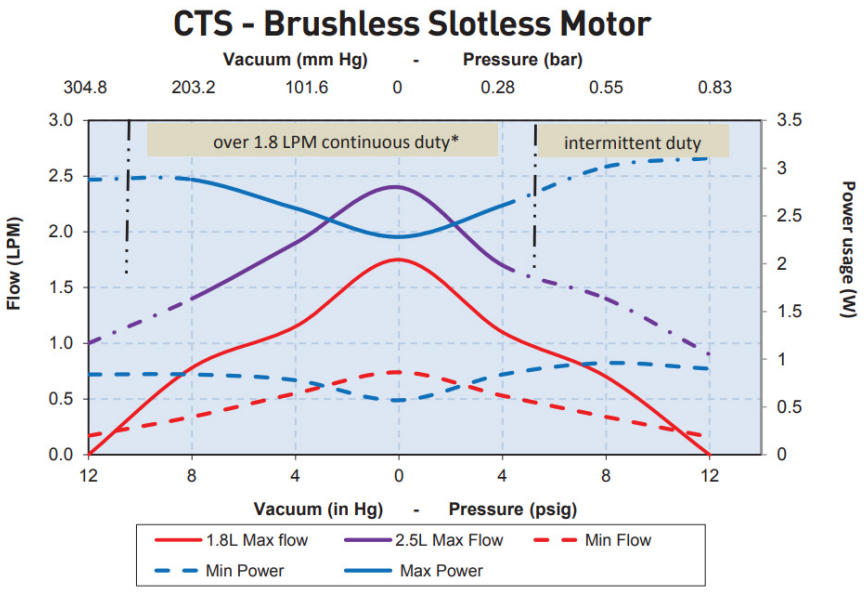

Figure 3.14. Flow rate performance of the Parker coreless CTS micro-diaphragm pump (E164-11-050) at 244 meters above sea level at 24°C in standard configuration (Parker Hannifin, 2015).

Flow and pressure parameters can be measured downstream of the ionization chamber (to avoid possible leakage), but before the pump (where the gas is ultimately released).

The Raspberry Pi (Type 3 Model B V1.2) receives power through a micro-usb connector (5 volts). All data logged from the pressure and flow sensors and the PID itself is logged on a micro-SD card on the Raspberry Pi. GPS data is also collected directly through the UAV. Code written in Python, adapted from Mathew Stewart (personal communication), is used to program the Raspberry Pi for data logging. A Waveshare 8 channel, 24 bit analog-to-digital converter (ADC) was mounted on the Raspberry Pi to process all the sensors' analog outputs.

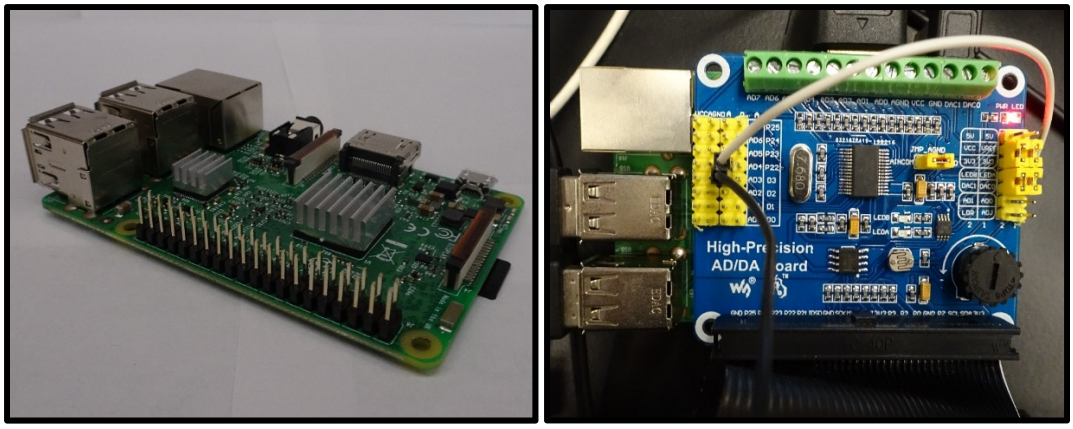

Figure 3.15. ***Left:*** *The Raspberry Pi used in the system. The black SD card sticks out on the far right.* ***Right:*** *The ADC mounted on top of the Raspberry Pi (on the front set of pins visible in the left image).*

3.3.4 PID Lamp

Resonance Ltd. built the lamp (model PID-KMD-EX) used. A 100-MHz RF exciter surrounds a Krypton filled lamp with a 1 mm thick MgF_2 window. A thin steel box enclosure provides shielding from the ensuing electromagnetic radiation to minimize noise on the other electronic components. The power supply with an EN3 electrical input powers both the exciter and a small cooling fan, operating at 24 volts and 2.71 amperes. The enclosure box is screwed directly onto the structural acrylic plate, securing not just the lamp but also the copper ionization chamber.

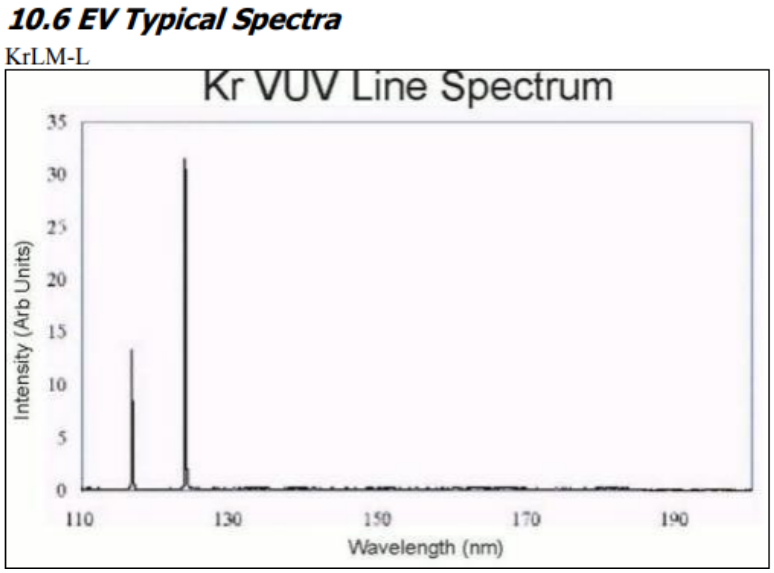

Figure 3.16. The typical emission spectra of the PID lamp. Emission occurs at 116.5 nm and 123.6 nm wavelengths, with 123.6 nm being the dominant one (10.6 e.v.) (Resonance Ltd., 2016).

The lamp outputs 10^{15} photons per second per steradian at two narrow wavelengths: 116.5 and 123.6 nm, as demonstrated in figure 3.16 above. For comparison, current top-of-the-line commercial sensors output a maximum of around 10^{12} or 10^{13} photons per second per steradian.

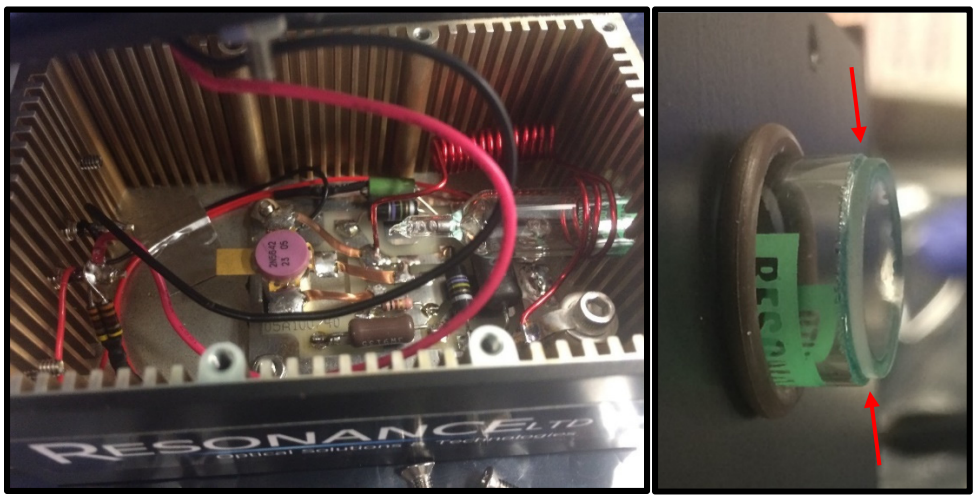

Figure 3.17. ***Left:*** *Internal view of the lamp's components. The bulb, on the far right, has a red RF coil around it. The wiring going upwards out of the image is for the cooling fan mounted in the roof (not pictured).* ***Right:*** *View after removing the steel protection plate on the surrounding bulb. It fits around the washer protecting the bulb, revealing only the window. The 1 mm thick MgF_2 window can be seen forming the tip of the bulb (red arrows).*

4. METHODS

4.1 Initial Sensor Testing and Calibration

In order to test for basic sensor functionality, several criteria were measured: flow rate consistency, electrical isolation, and signal response.

Flow rate consistency is tested by taking mass flow measurements at various points throughout the system, and particularly before and after leaving the ionization chamber. Even small leaks produce large distortions in signal response. This was controlled by using a Gilian Gilibrator-2 NIOSH primary standard air flow calibrator and comparing values to ensure consistency. The gilibrator contains bubble cells into which the air flows, and the length of time for a formed bubble to rise is measured and correlated to gas mass flow in cubic centiliters.

Electrical isolation is measured by applying various voltage biases (between 5 and 120 volts) across the copper pipe and rod, and by measuring that same voltage independently of the power source with the lamp turned off. With no ion generation, there should be no current, and thus electrical isolation between the plates. Agreement between the two readings confirms this.

Signal response provides confirmation of the sensor's functionality (but not sensitivity). An isopropyl alcohol source is placed near the gas inlet on the sensor, and instant immediate electric output provides confirmation that the sensor is responsive.

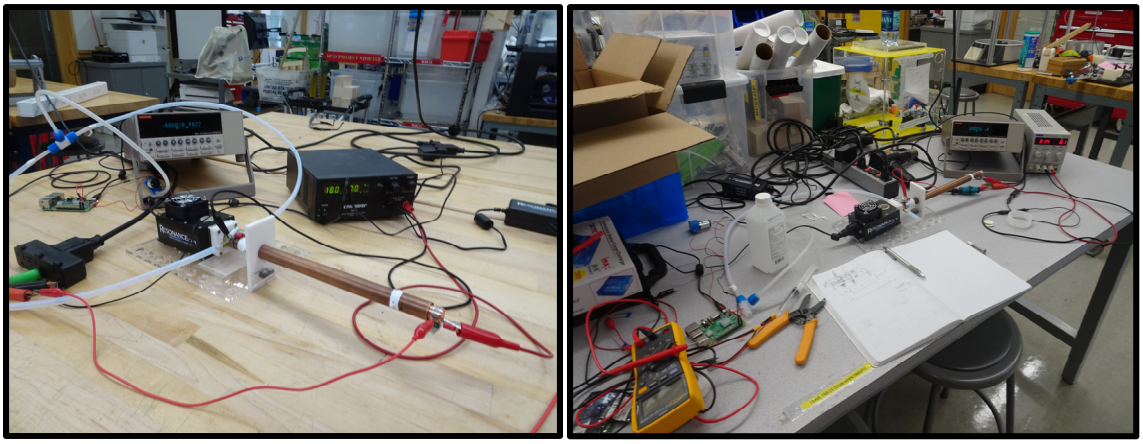

Figure 4.1. ***Left:*** *Initial electrical testing of the iteration 1 sensor design.* ***Right:*** *Testing for signal response in the iteration 1 sensor design with isopropyl alcohol.*

4.2 Laboratory Testing

Controlled laboratory tests were performed using standard gas samples. 1 ppm of alpha-pinene mixed with pure nitrogen gas was diluted with "pure air" to produce concentrations ranging between 1 and 20 ppb as necessary. Pure air was produced by an Aadco 737 pure air generator, and provides a standardized air composition, free from humidity, VOCs, or other trace compounds which could be ionized. Total pure air gas composition is comparable to atmospheric standards (nitrogen and oxygen concentrations, etc.). The pure air also flowed through a dry silica bead chamber for further humidity and VOC parameter control. Flow was controlled using MKS "Mass-Flo" air flow controllers with automated needle values through the National Instruments Labview evaluation software interface.

VOC concentrations followed a step model (figure 4.2), allowing for sensor cleansing between individual VOC measurements which increased accuracy by resetting the baseline measurement. Current measurements were made directly using a Keithley 6514 system electrometer. Using different time intervals (1, 2, and 5 minutes) for the

"steps", with all other factors held constant, allowed for response time evaluation, a crucial factor for practical use of the sensor. Following completion of successful design iteration 2 sensor testing, time intervals of 30 and 10 seconds were used on the iteration 3 sensor design with all other factors and experimental set-up components held constant as in earlier tests. Both alpha-pinene and isoprene testing was done.

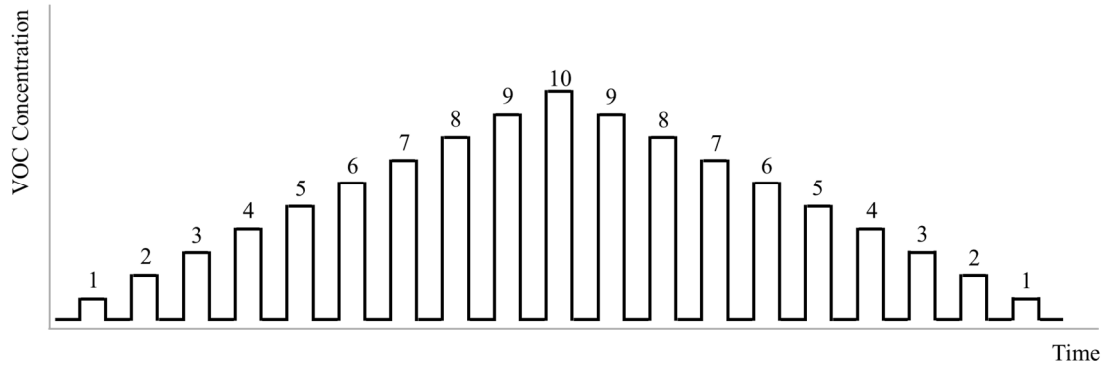

Figure 4.2. Step-wise experimental testing design. Different time intervals yield different width steps (longer times yield wider steps), allowing for response time testing. VOC concentrations typically ranged from 0 to 10 ppb. Making a measurement after flushing the sensor with 0 ppb VOC concentration air allows for increased accuracy by resetting the baseline.

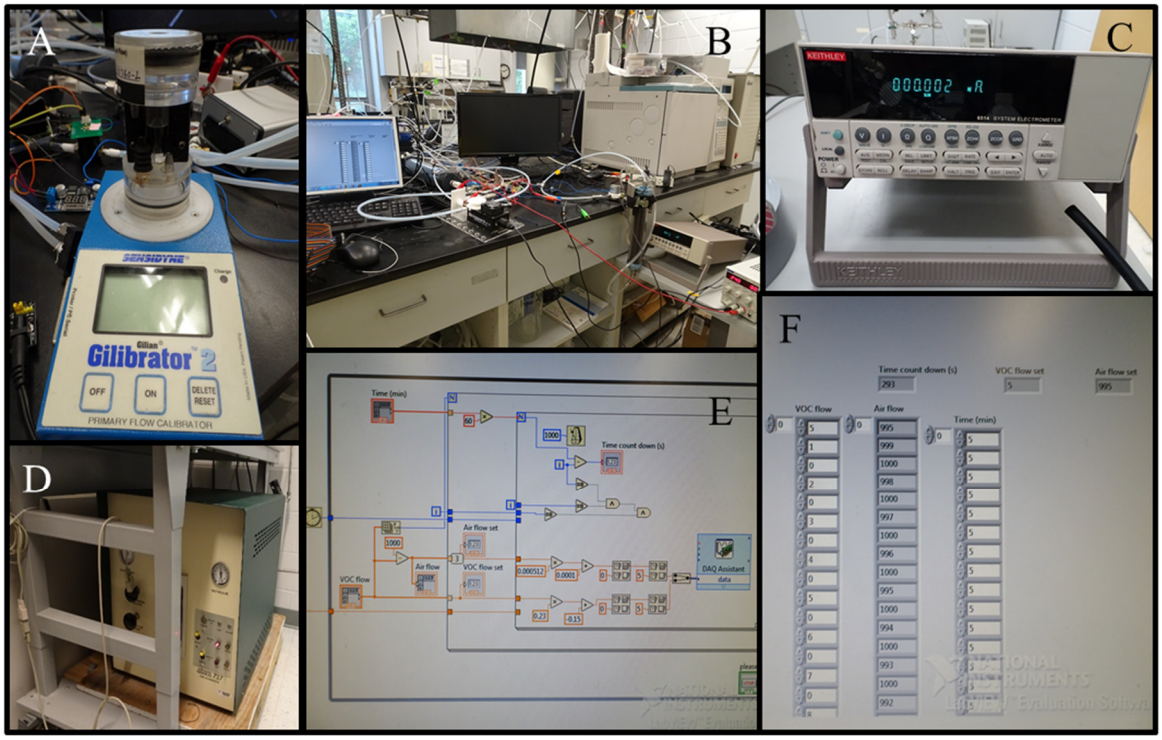

Figure 4.3. ***A****: The Gilian Gilibrator-2 NIOSH primary standard air flow calibrator with bubble chamber.* ***B****: Testing of the iteration 2 plate design sensor with alpha pinene in the laboratory, with data recording using the Keithley electrometer. In the bottom righthand corner both the power supply (red screen) and electrometer (blue/black screen) are visible.* ***C****: The Keithley 6514 system electrometer.* ***D****: The Aadco 737 pure air generator.* ***E****: back-end flow controller calibration interface for both pure air and concentrated VOCs during dilution.* ***F****: The front panel interface for controlling VOC concentrations.*

5. RESULTS AND DISCUSSION

5.1 Initial Sensor Tests and Proof of Concept

Results from the initial testing phase demonstrated that the design iteration 1 sensor was properly sealed using ferrules and PTFE sealant tape at all tubing junctions and connections by measuring air flow. Voltage was measured using a volt meter and electrical isolation confirmed between the copper rod and plate. However, the design iteration 1 sensor was insensitive to VOCs exposed at the original outlet, but, coincidently, the sensor was sensitive to VOC exposure at one of the gas outlets. Rather than intaking VOCs at the original long inlet with gas discharge through the two symmetric brass gas adapters, VOCs were up-taken through one of the brass adapters with discharge through only the single other original brass gas adapter, a design with which VOC signal response was successfully measured. Following this observation, the iteration 2, and later iteration 3, sensors were built, for which identical testing successfully took place.

5.2 Iteration 2 Sensor Testing

5.2.1 Laboratory Alpha-Pinene Testing

Alpha-pinene was used for the iteration 2 sensor design as alpha-pinene is more responsive than isoprene at 10.6 e.v. Step-wise results from the three step lengths—1, 2, and 5 minutes—are presented in figure 5.1. Raw current values in nanoamperes were collected, and average net change is presented (i.e., the average difference from 1 to 0, the average difference from 2 to 0, etc.). With shorter time intervals, the data is noticeably non-symmetric. This is indicative of "dead volume"—the VOC concentration of one step interferes with another. Thus, as VOC concentrations are increasing, they will appear lower than they actually are, and as VOC concentrations are decreasing, they will appear higher

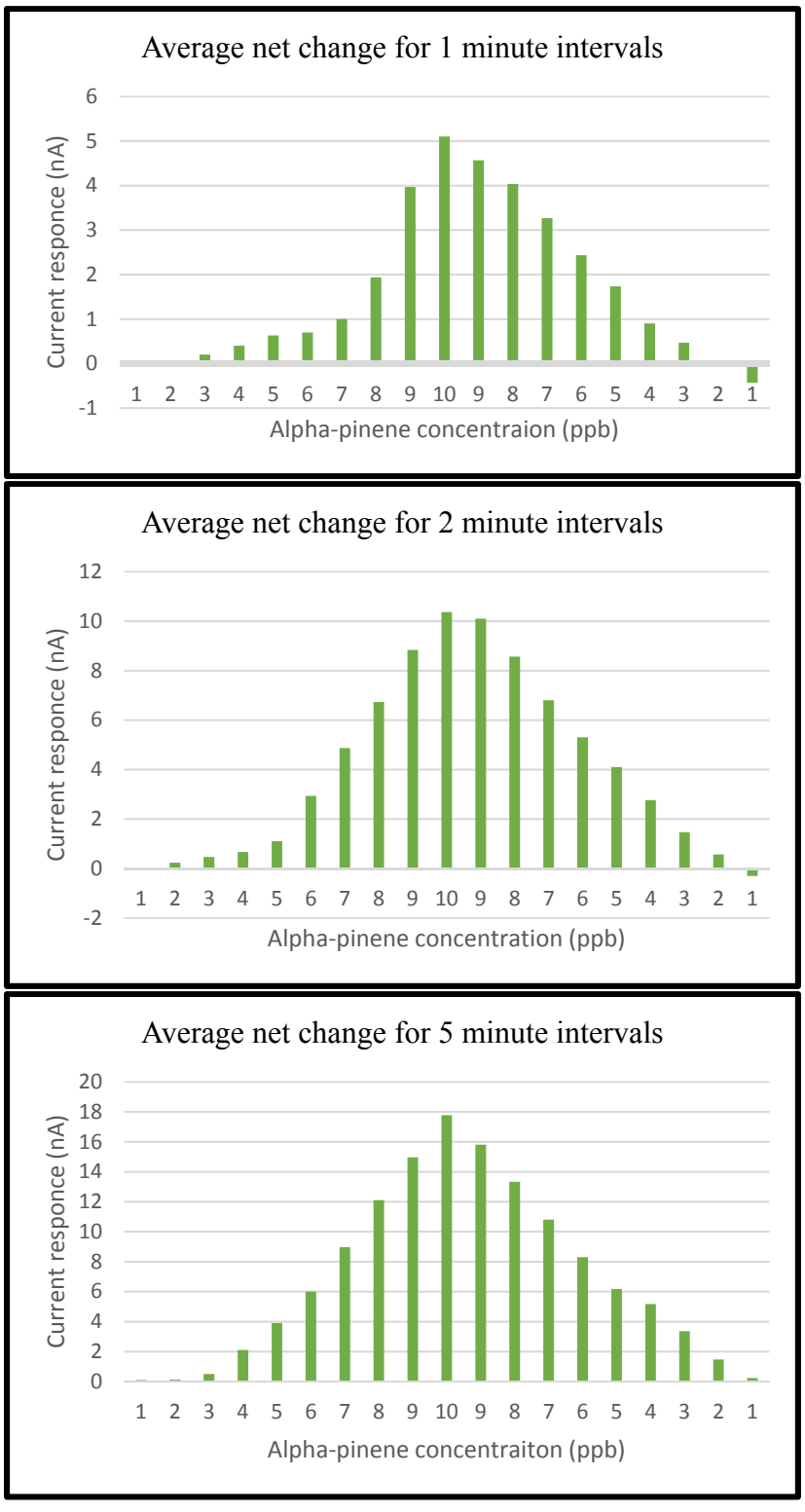

Figure 5.1. Average net changes in output current (in nanoamperes) during step testing at different time intervals (1, 2, and 5 minutes) for alpha-pinene with the plate design iteration 2 sensor. The non-symmetric shape indicates "dead-volume"—i.e., dependency of future measurements on current values. This is due to an incomplete flushing of the system, whereby gas of one VOC concentration is not fully removed before the next enters. This effect decreases with longer step times.

than they actually are, which is exactly what is seen in figure 5.1 (most dramatically in the 1-minute intervals). By having longer "steps", the air in the sensor may be fully flushed, or alternatively by increasing flow rate (increasing the absolute amount of gas of a given VOC concentration that has passed through the sensor before the reading is made). Due to the experimental set-up's particular calibration, increasing flow rate was more difficult than simply waiting longer to extend the "steps" during testing. Increasing the step time from 1 to 2 to 5 minutes provides a markedly more symmetric behavior. While even at 5-minute steps the measurements of the VOC concentration depend on the preceding value, this effect is clearly lower than for the previous shorter step trials (and is quantified statistically).

The average net change for 5-minute step interval trials provides the most conclusive demonstration of the PID's sensitivity. Response is generally measurable from 3 ppb upwards based on these measurements (figure 5.2). Additionally, long interval (24 hour) testing was done at low concentrations. Measurements of 1.7 nanoamperes at 0 ppb to 1.9 nanoamperes at 1 ppb, an increase of 0.2 nanoamperes, demonstrated that the PID is sensitive down to 1 ppb, but only at very these long-time intervals (not represented in figure 5.2). This sensitivity meets the sensitivity design criteria outlined in chapter 3, though response time is inadequate. With the Keithley electrometer able to resolve down to 10 attoamperes (10^{-18} amperes), with an accuracy of ± 3 femtoamperes (10^{-15} amperes), several magnitudes of order below the current sensor's measurements, it is possible to measure significantly smaller concentrations with the iteration 2 detector design. However, the current experimental system is not able to reliably produce sample gas concentrations below 1 ppb for measurement (as this would require a new method of producing pure air

and more flow controllers for further gas dilution). For the purposes of UAV-based atmospheric measurements, there can be additional challenges for such high-resolution measurements; the electrical shielding required for noise control could become prohibitive for mobile platforms, and the shared grounding could provide interference as well. Nonetheless, with the PID's sensitivity established, the next design iteration was meant to decrease dead volume and thus improve response time.

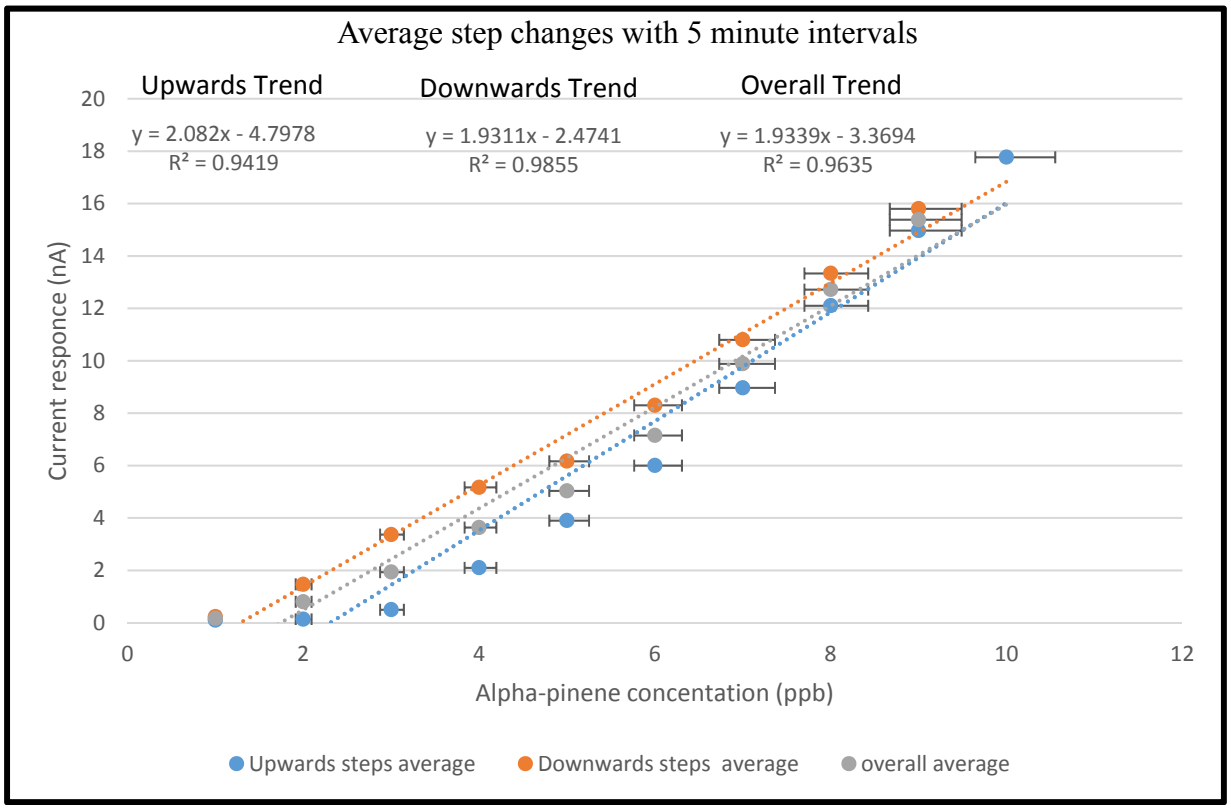

Figure 5.2. Overall average response of current to step changes in alpha-pinene concentration at 5-minute intervals with the plate design iteration 2 sensor (gray), average response of current to increasing step changes in alpha-pinene concentration (blue), and average response of current to decreasing step changes in alpha-pinene concentration (orange).

5.2.2 Statistical Analysis

Error was manually calculated by propagating all sources through the entire experimental setup. The alpha-pinene used was 1 ppm with accuracy better than 5%, calibrated with NIST traceable weights and supplied by Apel-Riemer Environmental in an

ultra-pure nitrogen mixture. The mass flow controller used for alpha-pinene (up to 20 standard cubic centimeters (sccm)) had an accuracy of ±1% full scale (FS) and the mass flow controller used for the dilution gas (up to 10000 sccm) had accuracy of ±1.5% FS. The electrometer's error with the setting used was ±0.1 nanoamperes. These errors were all used for calculating overall error as shown in figure 5.2. However, it is important to note there is significant uncertainty in the error—the actual error is likely much lower than that calculated and shown in the error bars; the values used were all extreme value guarantees provided by the manufacturers. Adding further possible uncertainty into the regression would increase bias and decrease the slope. However, Spearman's rank correlation coefficient is 1, providing strong evidence that there is no input error, meaning that certainty is high for the exact alpha-pinene concentration values used in the current regression.

Several statistical regressions were performed for the 5-minute interval trials. Overall an R^2 value of .96 demonstrates a fairly linear response, as PIDs are expected to follow. Indeed, through an f-test based on the Fisher–Snedecor distribution, the results were found to conform to the linear regression model. Additionally, a t-test, based on Student's t-distribution, was conducted to find p-values for all the trials (table 6). While fitting a second order polynomial, rather than a first order (linear) fit, does not immediately make sense for photoionization, it actually yields a useful picture. While PID responses may only be linear, a second order fit quantifies dead volume effects by incorporating preceding data measurements at each concentration. Thus, a sensor exhibiting some dead volume can be data-corrected to adjust for the contamination through t-testing. Additionally, the length of time necessary for "clean measurements" with the sensor can

be extrapolated by plotting the corrected quadratic terms, which decrease in trials with longer step intervals.

Table 6. T and P values for linear and quadratic fits across all testing step intervals with the iteration 2 sensor plate design for alpha-pinene testing.

Data	T-stat linear	T-stat quadradic	P-value linear	P-value quadradic
1-minute downwards average	17.18179	3.198229	5.55 E-07	0.018642
1-minute overall average	9.803503	6.58345	2.44 E-05	0.00059
1-minute upwards average	4.984899	5.750897	0.001073	0.000698
2-minute downwards average	26.00713	10.51179	3.17845 E-08	4.35435 E-05
2-minute overall average	11.4524	15.52205	8.69 E-06	4.52437 E-06
2-minute upwards average	8.338764	8.155788	3.24 E-05	8.06 E-05
5-minute downwards average	21.80072	5.360983	1.07825 E-07	0.001726504
5-minute overall average	13.59489	15.06712	2.74094 E-06	5.38732 E-06
5-minute upwards average	11.38448	9.49812	3.19906 E-06	3.00099 E-05

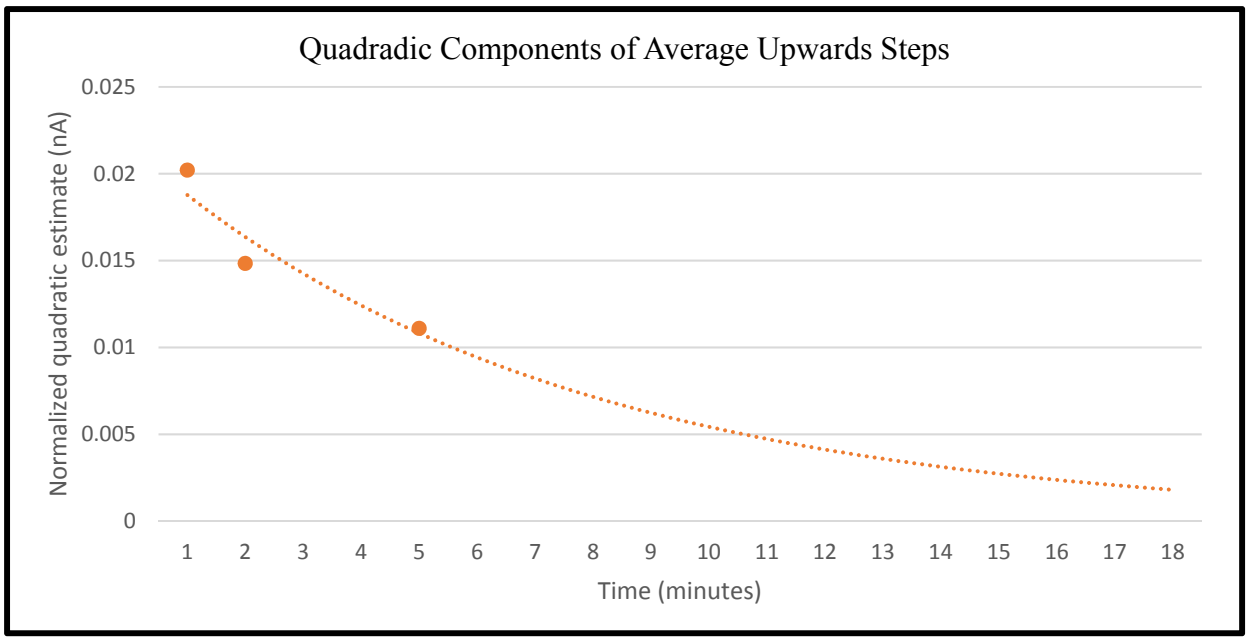

Figure 5.3. Normalized quadradic estimate terms from t-tests extrapolated to 18 minutes using an exponential function. These values can be used to data correct for dead volume and estimate the time step interval needed when dead volume will no longer be statistically significant.

The quadratic term is most prominent in VOC measurements during the increasing step phase, when dead-volume plays the most significant role (likely due to ambient conditions experienced before testing started). Normalizing the data points and plotting the quadratic estimate values produces the above graph, from which extrapolations and corrections can potentially be based. At about 17 minutes it can be expected that the quadratic term becomes statistically insignificant, at which point the response should be completely linear and there will be no effective dead volume (though the present experimental data at 5-minute intervals is already quite linear). Thus, if the design iteration 2 sensor is used in its current state, the quadratic terms can be subtracted to eliminate dead volume effects on the measurements (no data presented here has been adjusted though).

5.3 Iteration 3 Sensor Testing

5.3.1 Alpha-Pinene Testing

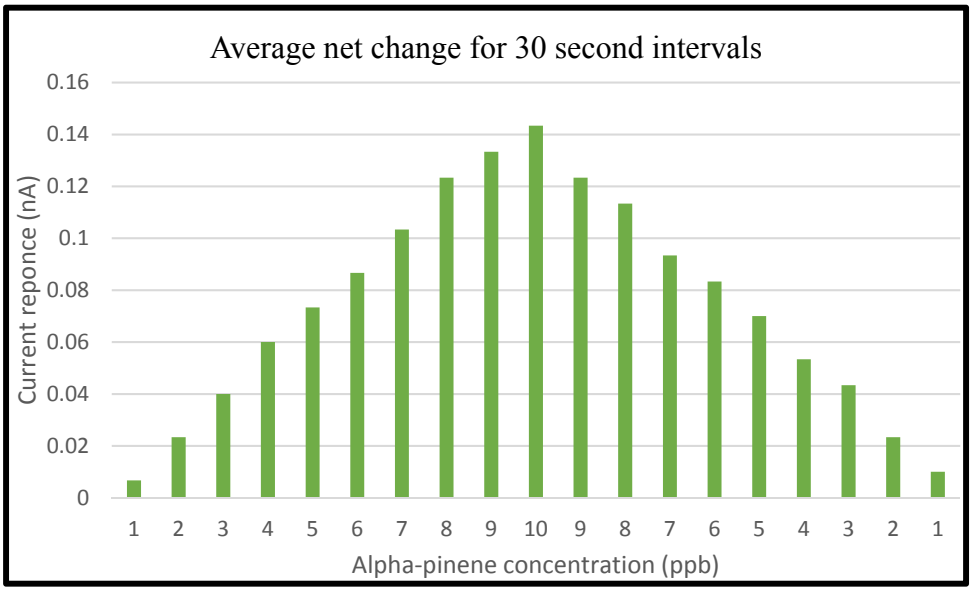

Figure 5.4. Average net changes in output current (in nanoamperes) during step testing at 30 second intervals for alpha-pinene with the iteration 3 plate design sensor. Comparing this with figure 5.1, dead-volume has been significantly reduced.

Following successful testing of the iteration 2 plate design sensor, the iteration 3 plate design was made to reduce dead volume and decrease response time. By decreasing ionization chamber length, modifying gas flow direction, and reducing the distance between the two plates, the chamber volume was reduced and stagnant air pockets were mostly eliminated. A response time improvement of several magnitudes was achieved as a result; the data given in figure 5.5 using the new design are significantly more linear than those in figure 5.2 with the older design, even though they were collected over step lengths 10 times shorter. However, it should be noted that the new design, while more reactive, is less sensitive. For equal changes in concentration the response current is significantly smaller. There is no physical explanation that relates the two behaviors, and so better design choices ought to allow the best of both sensor attributes with the next iteration. The

current design, while successfully minimizing dead volume, likely restricts optimal light transmission and hinders the ionization process; as a result, fewer ions are created and a smaller net current is produced. Nonetheless, enough sensitivity exists for successful and reliable 1 ppb detection capability.

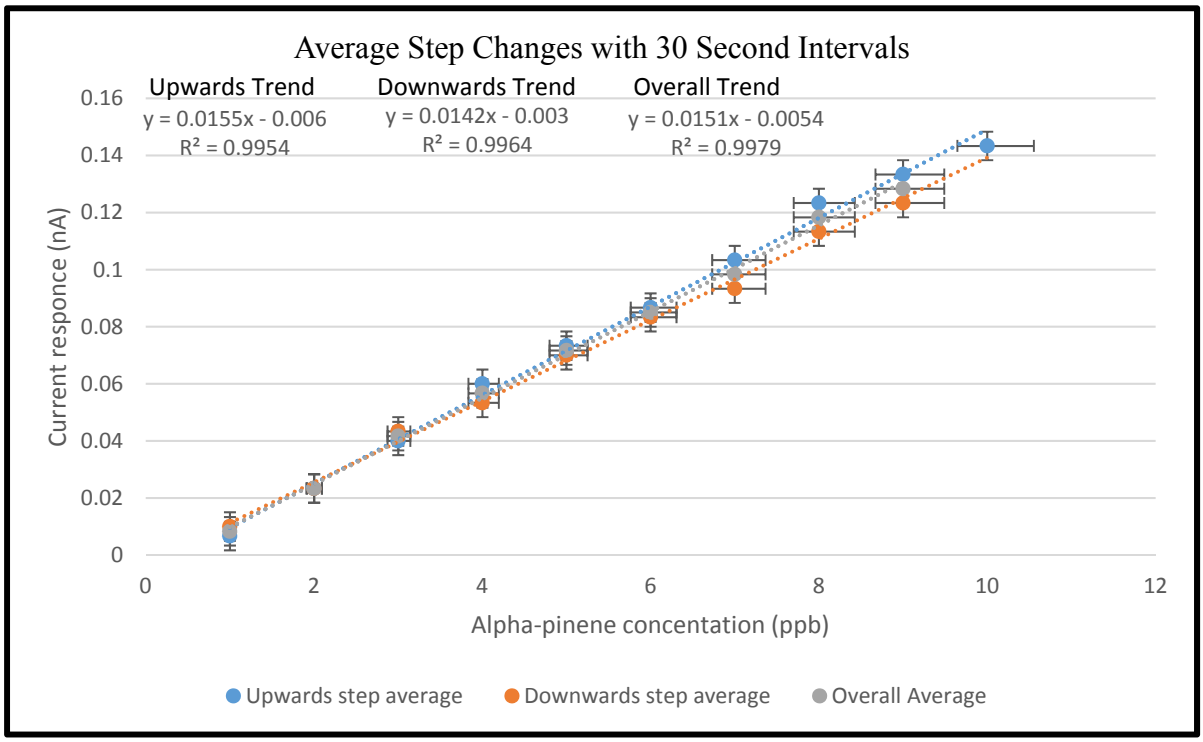

Figure 5.5. Overall average response of current to step changes in alpha-pinene concentration at 30 second intervals with the plate design iteration 3 sensor (gray), average response of current to increasing step changes in alpha-pinene concentration (blue), and average response of current to decreasing step changes in alpha-pinene concentration (orange). Compare with figure 5.2.

5.3.2 Isoprene Testing

Following successful completion of alpha-pinene testing, isoprene testing commenced using both 10 and 30 second interval steps. Isoprene is less responsive as compared to alpha-pinene at 10.6 e.v.s, so the response is less linear at 30 second steps compared to the alpha-pinene responses achieved in the previous testing. All other parameters were held constant.

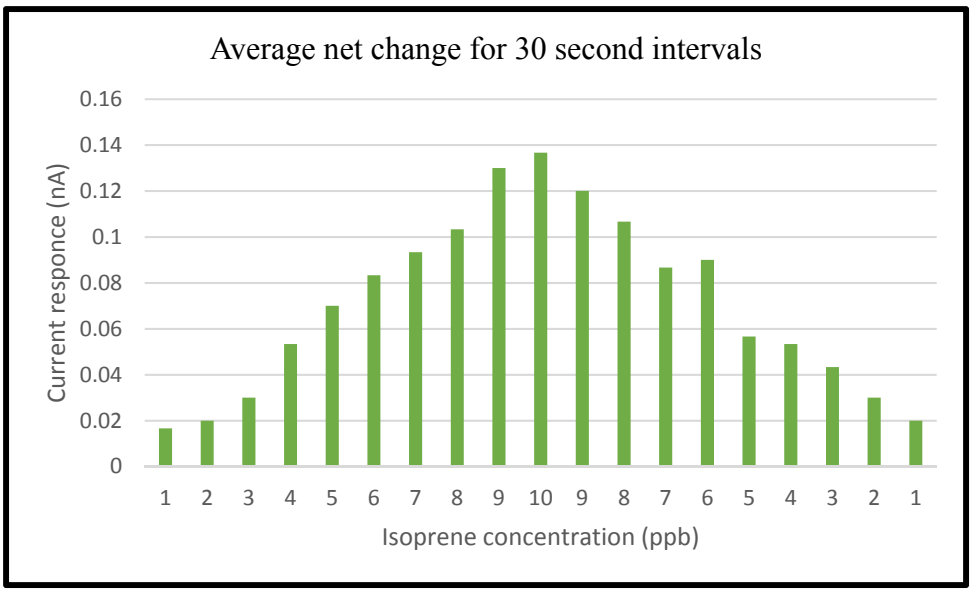

Figure 5.6. Average net changes in output current (in nanoamperes) during step testing at 30 second intervals for isoprene with the plate design iteration 3 sensor.

While the response is less linear (figure 5.7) compared to alpha-pinene, the sensor's sensitivity at low concentrations is greater for isoprene than for alpha-pinene.

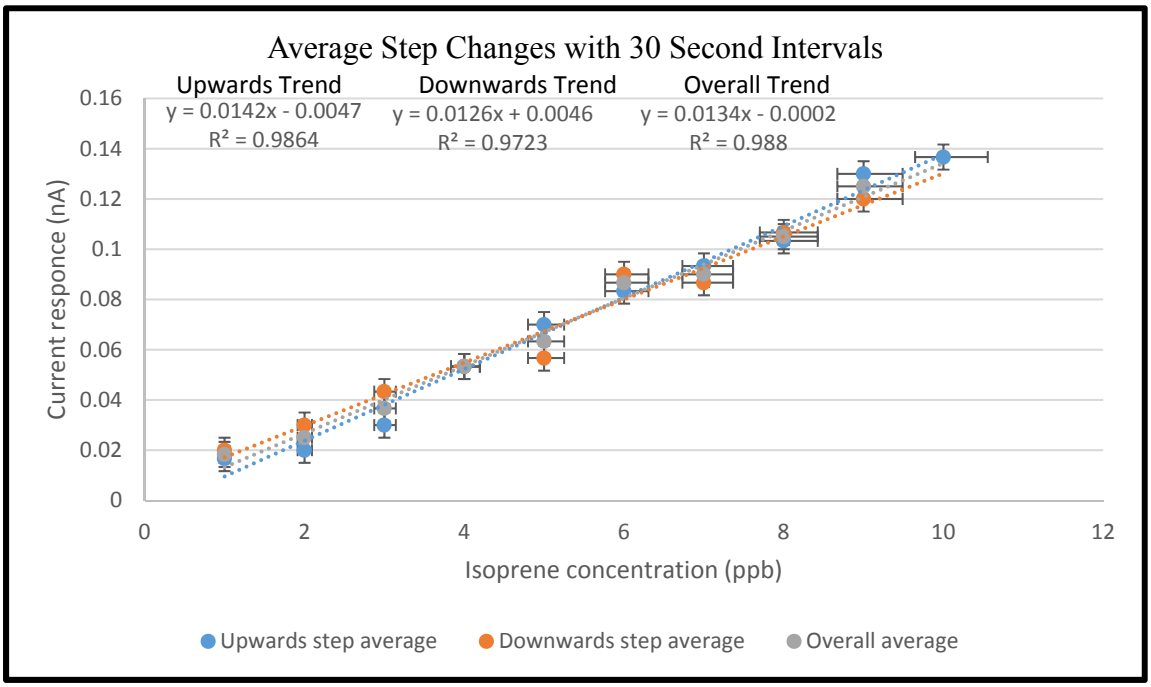

Figure 5.7. Overall average response of current to step changes in isoprene concentration at 30 second intervals with the plate design iteration 3 sensor (gray), average response of current to increasing step changes in isoprene concentration (blue), and average response of current to decreasing step changes in isoprene concentration (orange). Compare with figure 5.5.

In order to test at conditions likely to be most similar to those experienced by the UAV, rapid 10 second interval steps were also conducted using the iteration 3 sensor on isoprene gas. While there is slight loss of sensitivity at 1 ppb, the response is linear with little effect of possible dead volume despite the short time interval (figure 5.9).

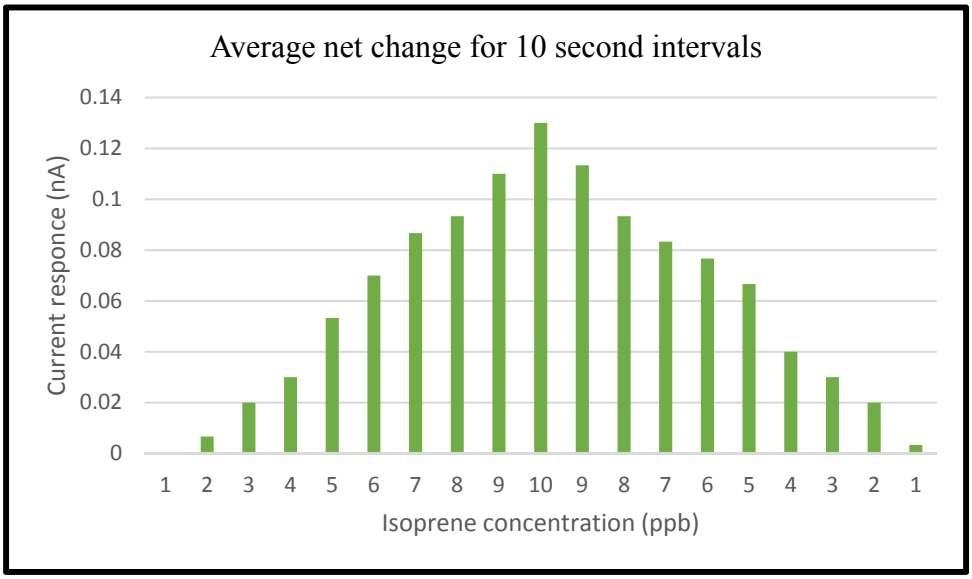

Figure 5.8. Average net changes in output current (in nanoamperes) during step testing at 10 second intervals for isoprene with the plate design iteration 3 sensor.

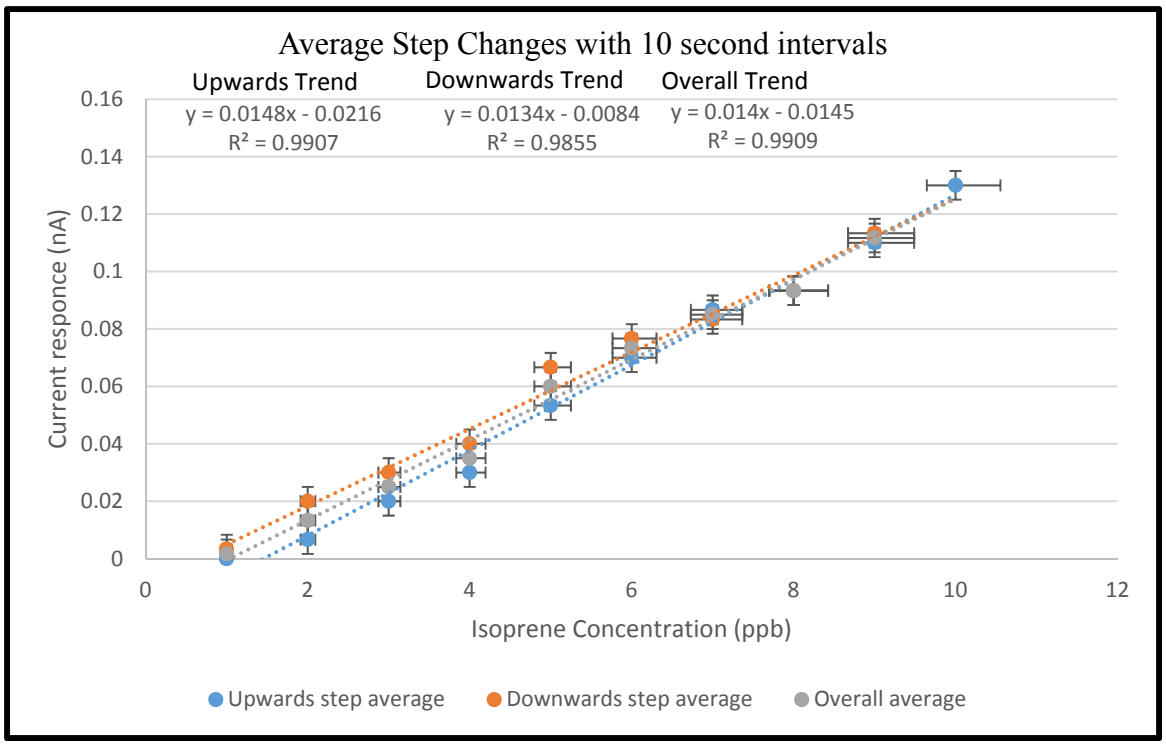

Figure 5.9. Overall average response of current to step changes in isoprene concentration at 10 second intervals with the plate design iteration 3 sensor (gray), average response of current to increasing step changes in isoprene concentration (blue), and average response of current to decreasing step changes in isoprene concentration (red). Compare with figure 5.7.

These data demonstrate that the PID in its current form (iteration 3) is highly sensitive to VOCs and operates at a response time appropriate for use on a UAV. While there are several parameters for clear improvement of the sensor, UAV-based, real-time measurements are now possible.

5.4 Summary of Sensor Iterations

Table 7 summarizes the results across all the sensors, and the different sensor iteration designs are shown side by side in figure 5.10. Dramatic improvements in sensitivity and portability characterize the improvement from the iteration 1 to iteration 2 plate designs, with a significant reduction in response time being the primary improvement from the iteration 2 to iteration 3 plate designs.

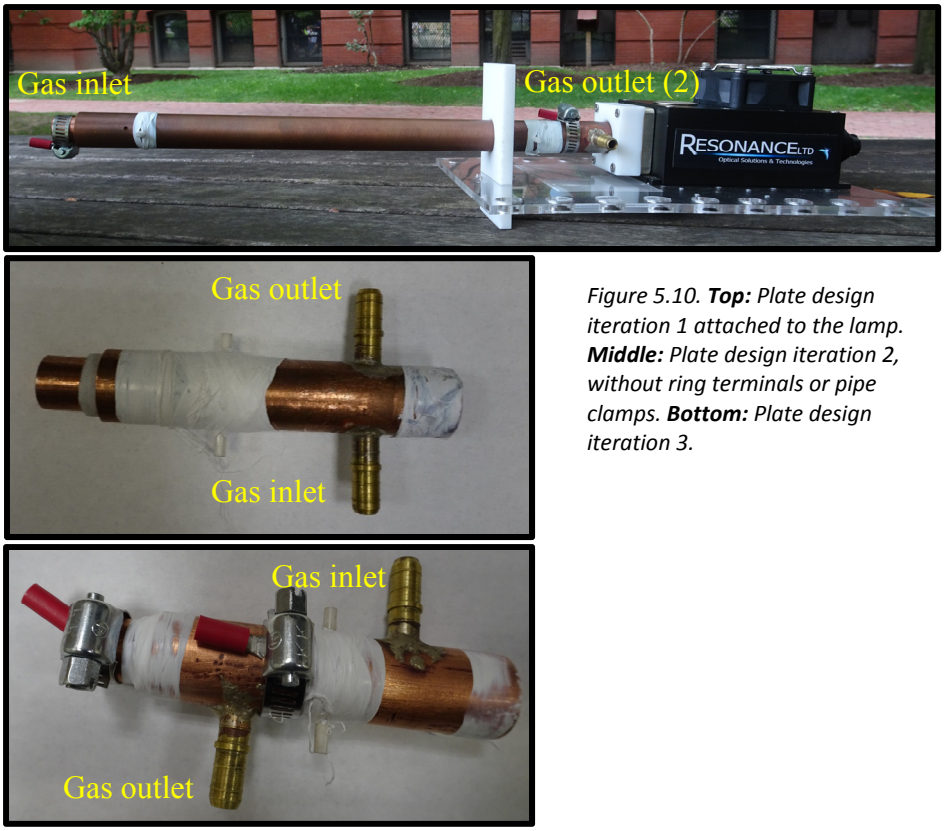

Figure 5.10. ***Top:*** *Plate design iteration 1 attached to the lamp.* ***Middle:*** *Plate design iteration 2, without ring terminals or pipe clamps.* ***Bottom:*** *Plate design iteration 3.*

Table 7. Summary of results.

	Top Sensitivity	Response Time	Portability	Major Changes
Sensor Iteration 1	Signal response only to ppm levels	N/A	Heavy sensor, able to be mounted on drone, but would probably not be successful in flight.	First successfully built sensor.
Sensor Iteration 2	At a "practical" time response, 3 ppb	5 minutes	Drone mountable and of appropriate weight.	Flow direction changed to be perpendicular across lamp, ionization chamber shortened.
Sensor Iteration 3	1 ppb detection	Decreased to 10 seconds	Similar to sensor iteration 3, slightly lighter.	Dead volume decreased, plate distance narrowed, gas outlet moved farther from gas inlet.

5.5 Overall Assembly on the Hexacopter UAV

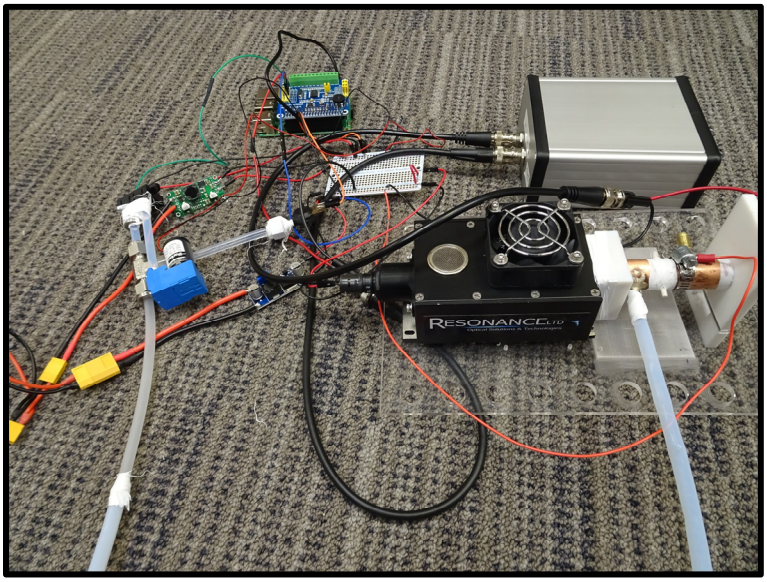

Figure 5.11. All components of the sensor system before being mounted on the UAV.

All electronic components were soldered using lead-based solder following the schematic developed in figure 3.13. All gas flow sensors were connected using PTFE tubing and sealed using PTFE tape. The acrylic plate on which the lamp was mounted was attached on the undercarriage of the UAV using 4 zip ties. All electronic components were tightly mounted in the space between the acrylic plate and the UAV's undercarriage.

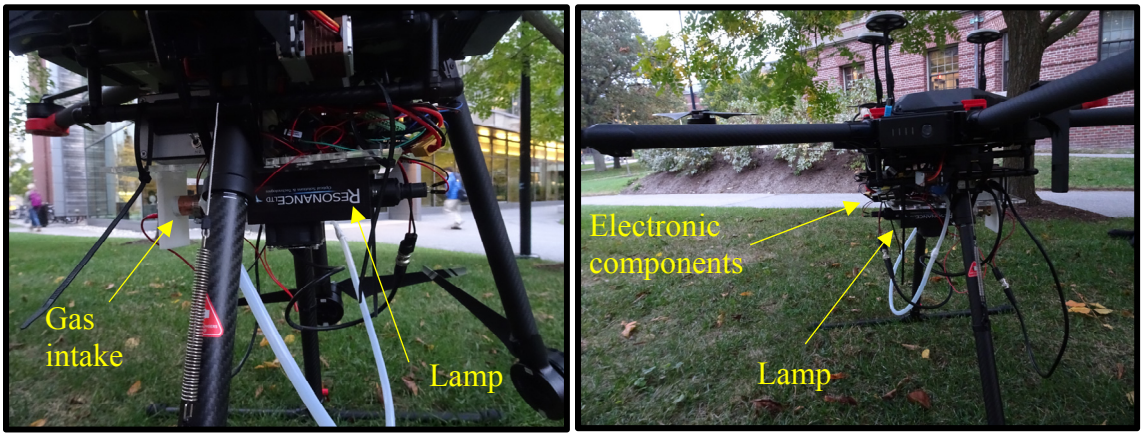

Figure 5.12. Side views of the mounted sensor system. Gas intake occurs at the left of the UAV (yellow arrow), and the lamp is on the right. All electronics are mounted on top of the lamp above the acrylic plate.

Figure 5.13. Front view of the final complete design iteration 3 sensor system mounted on the UAV.

6. CONCLUSIONS

This thesis demonstrates that a photoionization sensor, sensitive up to 1 ppb VOC concentrations, has been successfully developed and mounted on a UAV, with sensitivity and time response meeting the design criteria specified. The PID sensor system mounts on the drone at a total weight of 1.68 kg with physical dimensions of about 24 cm in length by 16 cm in width by 15 cm in height. While further testing is needed to develop precise correlation curves between various VOC concentrations and output voltage for use of the sensor in data collection during field use, the current sensor (iteration 3) is ready for trials for field applications and laboratory use. The current model is usable at concentrations around 1 ppb with a rapid response time (10 seconds) and may be fully powered using the UAV's power supply. Flow rate and air pressure can be recorded alongside current output.

Further steps include supplementary testing in both laboratory and field settings, as well as additional optimization of the sensor system. Table 8 presents possible further steps to be taken, in order of top priority.

Table 8. Possible future steps in order of priority.

Further Modification	Added Benefits	Implementation Challenges and Feasibility
Establishing PID sensitivity below 1 ppb in the parts per trillion (ppt) range through improvements in design of the detector plates and ionization chamber	The iteration 4 design can be made more sensitive, lighter, and smaller.	Modifications will be necessary to the current laboratory testing setup to permit ppt concentrations of VOC gas flow for testing. Construction of the design iteration 4 sensor, drawing upon the iteration 2 and 3 designs, will be necessary.
Further optimization of the TIA in the sensor system to permit for practical data collection during flight.	The TIA can be modified to be more sensitive, more compatible with current PID testing systems, smaller, and lighter.	It will be necessary to change a resistor in the current TIA, perform further laboratory testing, and modify the current electric shielding box.
Coupling the PID with VOC selectivity and humidity control mechanisms.	Not only total VOC concentrations can be measured, but specifically C5 (for example) compounds can be selected for. Humidity and temperature can be corrected for through data adjustment or gas pre-treatment.	Coupling of the current sensor with a pretreatment chamber, where certain compounds are absorbed (certain unwanted VOCs, water molecules, etc.) is necessary.
Gold plating the detector plates.	Increased lifespan and accuracy of the PID (by avoiding oxidation of copper).	The design iteration 4 plates need to be sputter coated or electroplated with gold, a straightforward procedure.
Laboratory testing of VOC mixtures.	More realistic laboratory testing of VOCs, with increased similarity to those mixtures likely to be encountered in the field.	It is necessary to change VOC gas cylinders currently being used in laboratory testing.

Field testing of the sensor system.	Useful collection of data exploring short lived VOCs, possible super emitters, and biogenic VOC emission inventories.	Organization of a sampling campaign in an area such as the Amazon is needed.
MOSFET switch implementation on the breadboard.	Better accuracy and data correction for the produced ion current in the PID by permitting rapid on/off power switching of the lamp.	Adding a few electronic elements to the sensor system's central breadboard and modifying the Raspberry Pi code is needed.
Implementation of wireless data transmission.	Possibility for not just real-time data collection, but also real-time data analysis.	Implementing an on-board SIM card coupled to the Raspberry Pi or using the drone's flight control channels also for data transmission is necessary.

The new sensor demonstrates the feasibility of onboard, real-time VOC measurements on UAVs, a revolutionary advantage when compared to current testing methods. This technology allows for bias reduction in global biogenic VOC measurements permitting more accurate global climate models and provides a proof of concept for a new technique for future field data collection.

7. REFERENCES

Allen, J. L. *et al.* (2014) 'Early Postnatal Exposure to Ultrafine Particulate Matter Air Pollution: Persistent Ventriculomegaly, Neurochemical Disruption, and Glial Activation Preferentially in Male Mice', *Environmental Health Perspectives*, 122(9), pp. 939–945.

American Thoracic Society (2017) *Air pollution a concern at levels currently accepted as 'safe'*, *ScienceDaily*.

Anenberg, S. C. *et al.* (2010) 'An Estimate of the Global Burden of Anthropogenic Ozone and Fine Particulate Matter on Premature Human Mortality Using Atmospheric Modeling', *Environmental Health Perspectives*, 118(9), pp. 1189–1195. doi: 10.1289/ehp.0901220.

Apte, J. S. *et al.* (2018) 'Ambient PM 2.5 Reduces Global and Regional Life Expectancy', *Environmental Science & Technology Letters*. American Chemical Society, 5(9), pp. 546–551. doi: 10.1021/acs.estlett.8b00360.

Arden Pope III, C., Ezzati, M. and Dockery, D. W. (2009) 'Fine-Particulate Air Pollution and Life Expectancy in the United States', *The New England Journal of Medicine*, 360(4), pp. 376–386.

Armendáriz-arnez, C. *et al.* (2010) 'Indoor particle size distributions in homes with open fires and improved Patsari cook stoves', *Atmospheric Environment*. Elsevier Ltd, 44(24), pp. 2881–2886. doi: 10.1016/j.atmosenv.2010.04.049.

Atkinson, R. and Arey, J. (2003) 'Atmospheric Degradation of Volatile Organic Compounds', *Chemical Reviews*, 103(12), pp. 4505–4638. doi: 10.1021/cr0206420.

Banerjee, A. and Sharkey, T. D. (2014) 'Methylerythritol 4-phosphate (MEP) pathway metabolic regulation', *Natural Product Reports*, (8), pp. 1043–1055. doi: 10.1039/c3np70124g.

Barregard, L. *et al.* (2006) 'Experimental Exposure to Wood-Smoke Particles in Healthy Humans : Effects on Markers of Inflammation , Coagulation , and Lipid Peroxidation Experimental Exposure to Wood-Smoke Particles in Healthy Humans : Effects on Markers of Inflammation , Coagulation', *Inhalation Toxicology*, 18(11), pp. 845–853. doi: 10.1080/08958370600685798.

Bateson, T. F. and Schwartz, J. (2004) 'Who is Sensitive to the Effects of Particulate Air Pollution on Mortality ? A Case-Crossover Analysis of Effect Modifiers', *Epidemiology*, 15(2), pp. 143–149. doi: 10.1097/01.ede.0000112210.68754.fa.

Batista, C. E. *et al.* (2019) 'Intermediate-scale horizontal isoprene concentrations in the near-canopy forest atmosphere and implications for emission heterogeneity', *PNAS*, 116(39), pp. 19318–19323. doi: 10.1073/pnas.1904154116.

Bauleo, L. *et al.* (2019) 'Long-term exposure to air pollutants from multiple sources and mortality in an industrial area : a cohort study', *Occupational and Environmental Medicine*, 76(1), pp. 48–57. doi: 10.1136/oemed-2018-105059.

Bonn, B. *et al.* (2018) 'Impact of vegetative emissions on urban ozone and biogenic secondary organic aerosol: Box model study for Berlin, Germany', *Journal of Cleaner Production*, 176, pp. 827–841. doi: 10.1016/j.jclepro.2017.12.164.

Bos, I. *et al.* (2014) 'Physical Activity , Air Pollution and the Brain', *Sports Medicine*, 44(11), pp. 1505–1518. doi: 10.1007/s40279-014-0222-6.

Ten Brinke, J. *et al.* (1998) 'Development of New Volatile Organic Compound (VOC) Exposure Metrics and their Relationship to "' Sick Building Syndrome '" Symptoms', *Indoor Air*, 8(510), pp. 140–152.

Brook, R. D. (2007) 'Is Air Pollution a Cause of Cardiovascular Disease ? Updated Review and Controversies', *Reviews on Environmental Health*, 22(2), pp. 115–138.

Broughton, E. (2005) 'The Bhopal disaster and its aftermath : a review', *Environmental Health*, 6(4), pp. 1–6. doi: 10.1186/1476-069X-4-6.

Burney, J. and Ramanathan, V. (2014) 'Recent climate and air pollution impacts on Indian agriculture', *PNAS*, 111(46), pp. 16319–16324. doi: 10.1073/pnas.1317275111.

California OEHHA (2003) *Air Pollution and Children's Health*.

Carlo, P. Di *et al.* (2004) 'Missing OH Reactivity in a Forest : Evidence for Unknown Reactive Biogenic VOCs', *Science*, 304(5671), pp. 722–726.

Carter, W. P. L. (1994) 'Development of Ozone Reactivity Scales for Volatile Organic Compounds', *Air & Waste*, 44(7), pp. 881–899. doi: 10.1080/1073161X.1994.10467290.

Catcott, E. J. (1961) 'Effects of Air pollution on Animals', *World Health Organization monograph series on air pollution*, (46), pp. 221–232.

Chameides, W. L. *et al.* (1999) 'Is Ozone Pollution Affecting Crop Yields in China', *Geophysical Research Letters*, 26(7), pp. 867–870.

Cohen, A. J. *et al.* (2006) 'The Global Burden of Disease Due to Outdoor Air Pollution', *Journal of Toxicology and Environmental Health, Part A*, 7394(68), pp. 1301–1307. doi: 10.1080/15287390590936166.

Cox, B. *et al.* (2017) 'Ambient Air Pollution-Related Mortality in Dairy Cattle : Does It Corroborate Human Findings ?', *Epidemiology*, 27(6), pp. 779–786. doi: 10.1097/EDE.0000000000000545.Ambient.

Danaei, G. *et al.* (2005) 'Causes of cancer in the world : comparative risk assessment of nine behavioural and environmental risk factors', *The Lancet*, 366(9499), pp. 1784–1793.

DeSombre, E. R. (2000) 'The Experience of the Montreal Protocol : Particularly Remarkable , and Remarkably Particular', *UCLA Journal of Environmental Law and Policy*, 19(1), pp. 49–82.

Devine, E. *et al.* (2014) 'Development and Testing of a Field Screening Method Based on Bubbling Extraction and Photoionization Detection for Measurement of Benzene and Total VOCs', *Groundwater Monitoring and Remediation*, 34(3), pp. 95–104. doi: 10.1111/gwmr.12070.

Devlin, R. B. *et al.* (2012) 'Controlled Exposure of Healthy Young Volunteers to Ozone Causes Cardiovascular Effects', *Circulation*, 126(1), pp. 104–111. doi: 10.1161/CIRCULATIONAHA.112.094359.

Driscoll, J. N. (1977) 'Evaluation of a new photoionization detector for organic compounds', *Journal of Chromatography*, 134(1), pp. 49–55.

Edgerton, S. A. *et al.* (1989) 'Inter-Urban Comparison of Ambient Volatile Organic Compound Concentrations in U.S. Cities', *Air and Waste*, 39(5), pp. 729–732. doi: 10.1080/08940630.1989.10466561.

Fenger, J., Hertel, O. and Palmgren, F. (1998) *Urban Air Pollution - European Aspects*. Dordrecht: Springer Science+Business Media Dordrecht.

Ferkol, T. and Schraufnagel, D. (2014) 'The Global Burden of Respiratory Disease', *Annals of the American Thoracic Society*, 11(3), pp. 404–406. doi: 10.1513/AnnalsATS.201311-405PS.

Folinsbee, L. J. (1992) 'Human Health Effects of Air Pollution', *Environmental Health Perspectives*, 100(12), pp. 45–56.

Freedman, A. N. (1982) 'Photoionization Detector Response', *Journal of Chromatography*, 236, pp. 11–15.

George, I. J. and Abbatt, J. P. D. (2010) 'Heterogeneous oxidation of atmospheric aerosol particles by gas-phase radicals', *Nature Chemistry*. Nature Publishing Group, 2(SEPTEMBER), pp. 713–722. doi: 10.1038/nchem.806.

Gordin, M. D. . (1997) 'The Anthrax Solution : The Sverdlovsk Incident and the Resolution of a Biological Weapons Controversy', *Journal of the History of Biology*, 30(3), pp. 441–480.

Granier, C. *et al.* (2011) 'Evolution of anthropogenic and biomass burning emissions of air pollutants at global and regional scales during the 1980 – 2010 period', *Climatic Change*, 109(163), pp. 163–190. doi: 10.1007/s10584-011-0154-1.

Griffin, J., Cocker, D. R. and Seinfeld, H. (1999) 'Estimate of global atmospheric organic aerosol from oxidation of biogenic hydrocarbons', *Geophysical Research Letters*, 26(17), pp. 2721–2724.

Gruijl, F. R. De and Leun, J. C. Van Der (2000) 'Environment and health: 3. Ozone depletion and ultraviolet radiation', *CMAJ*, 163(7), pp. 851–855.

Guenther, A. *et al.* (1995) 'A global model of natural volatile organic compound emissions s Triangle Exposure Assessment Science and These inventories', *Journal of Geophysical Research*, 100(D5), pp. 8873–8892. doi: 10.1029/94JD02950.

Guimaraes, P. *et al.* (2019) 'Vertical Profiles of Ozone Concentration Collected by an Unmanned Aerial Vehicle and the Mixing of the Nighttime Boundary Layer over an Amazonian', *Atmosphere*, 599(10), pp. 1–14.

Haszpra, L. *et al.* (2015) 'How well do tall-tower measurements characterize the CO 2 mole fraction distribution in the planetary boundary layer ?', *Atmospheric Measurement Techniques*, 8, pp. 1657–1671. doi: 10.5194/amt-8-1657-2015.

Henze, D. K. and Seinfeld, J. H. (2006) 'Global secondary organic aerosol from isoprene oxidation', *Geophysical Research Letters*, 33(May), pp. 6–9. doi: 10.1029/2006GL025976.

Hewitt, C. N. *et al.* (1993) 'Atmospheric VOCs from natural sources', *Volatile Organic Compounds in the Atmosphere*, pp. 17–36. doi: 10.1039/9781847552310-00017.

Holopainen, J. K. and Gershenzon, J. (2010) ‘Multiple stress factors and the emission of plant VOCs’, *Trends in Plant Science*. Elsevier Ltd, 15(3), pp. 176–184. doi: 10.1016/j.tplants.2010.01.006.

Ioffe, B. V, Isidorov, V. A. and Zenkevich, I. G. (1977) ‘Gas chromatographic-mass spectrometric determination of volatile organic compounds in an urban atmosphere’, *Journal of Chromatography*, 142, pp. 787–795.

Ion Science (2017) *MiniPID 2 (3PIN) Instument User Manual V1.3R*.

Ion Science (2019) ‘Technical / Application Article 02’, p. 16.

Ito, K. *et al.* (1992) ‘Associations of London, England, Daily Mortality with Particulate Matter, Sulfur Dioxide, and Acidic Aerosol Pollution’, *Archives of Environmental Health: An International Journal*, 48(4), pp. 213–220.

Jacob, D. (1999) *Atmospheric Chemistry*. 1st edn. Princeton: Princeton University Press.

Jacob, J. D. *et al.* (2018) ‘Considerations for Atmospheric Measurements with Small Unmanned Aircraft Systems’, *Atmosphere*, 9(7)(252), pp. 1–16. doi: 10.3390/atmos9070252.

Jimenez, J. L. *et al.* (2009) ‘Evolution of Organic Aerosols in the Atmosphere’, *Science*, 326(5959), pp. 1525–1530.

Johnson, J. (2008) ‘Selection of Materials for UV Optics’, (2), pp. 1–6.

Jones, N. (2001) ‘The nose and paranasal sinuses physiology and anatomy’, *Advanced Drug Delivery Reviews*, 51(1–3), pp. 5–19.

Kampa, M. and Castanas, E. (2008) ‘Human health effects of air pollution’, *Environmental Pollution*, 151(2), pp. 362–367. doi: 10.1016/j.envpol.2007.06.012.

Kanakidou, M. *et al.* (2005) ‘Organic aerosol and global climate modelling : a review’, *Atmospheric Chemistry and Physics*, 5, pp. 1053–1123.

Kesselmeier, J. *et al.* (2002) ‘Volatile organic compound emissions in relation to plant carbon fixation and the terrestrial carbon budget’, *Global Geochemical Cycles*, 16(4), pp. 1–9. doi: 10.1029/2001GB001813.

Kim, B. R. (2011) ‘VOC Emissions from Automotive Painting and Their Control : A Review’, *Environmental Engineering Research*, 16(1), pp. 1–9. doi: 10.4491/eer.2011.16.1.001.

Koppmann, R. (2007) *Volatile Organic Compounds in the Atmosphere*. Blackwell Publishing.

Kumar, P. *et al.* (2014) ‘Ultra fine particles in cities’, *Environment International*, 66(May), pp. 1–10. doi: 10.1016/j.envint.2014.01.013.

Langhorst, M. L. (1981) ‘Photoionization Detector Sensitivity of Organic Compounds’, *Journal of Chromatographic Science*, 19(2), pp. 98–103.

Laothawornkitkul, J. *et al.* (2009) ‘Biogenic volatile organic compounds in the Earth system’, *New Phytologist*, 183, pp. 27–51.

Leaf, A. (1993) *Loss of Stratospheric Ozone and Health Effects of Increased Ultraviolet Radiation*, *Critical condition: Human health and environment*. Edited by E. Chivian et al. Cambridge, MA: The MIT Press.

Ledford, D. K. and Lockey, R. F. (1994) 'The journal of Allergy and clinical immunology', *The journal of Allergy and clinical immunology*, 94(2.2), pp. 275–276.

Lee, D. S., Holland, M. R. and Falla, N. (1996) 'The Potential Impact of Ozone on Materials in the U.K.', *Atmospheric Environment*, 30(7), pp. 1053–1065.

Lelieveld, J. *et al.* (2015) 'The contribution of outdoor air pollution sources to premature mortality on a global scale', *Nature*, 525, pp. 367–371. doi: 10.1038/nature15371.

Leung, D. Y. C. (2015) 'Outdoor-indoor air pollution in urban environment : challenges and opportunity', *Frontiers in Environmental Science*, 2(January), pp. 1–7. doi: 10.3389/fenvs.2014.00069.

Lilllie, R. (1972) *AIR POLLUTANTS AFFECTING THE PERFORMANCE OF DOMESTIC ANIMALS AIR POLLUTANTS AFFECTING THE PERFORMANCE OF DOMESTIC ANIMALS*. Washington D.C.: Agricultural Research Service, United States Department of Agriculture.

Lippmann, M. (1989) 'HEALTH EFFECTS OF OZONE', *JAPCA*, 39(5), pp. 672–695. doi: 10.1080/08940630.1989.10466554.

Logan, W. P. D. (1953) 'Mortality in the London Fog Incident, 1952', *The Lancet*, 261(6755), pp. 336–338.

Lu, X. *et al.* (2016) 'Source apportionment and health effect of NO x over the Pearl River Delta region in southern China', *Environmental Pollution*. Elsevier Ltd, 212(May), pp. 135–146. doi: 10.1016/j.envpol.2016.01.056.

Matsumoto, J. (2014) 'Measuring Biogenic Volatile Organic Compounds (BVOCs) from Vegetation in Terms of Ozone Reactivity', *Aerosol and Air Quality Research*, 14, pp. 197–206. doi: 10.4209/aaqr.2012.10.0275.

Mauzerall, D. L. *et al.* (2005) 'NO x emissions from large point sources : variability in ozone production , resulting health damages and economic costs', *Atmospheric Environment*, 39(16), pp. 2851–2866. doi: 10.1016/j.atmosenv.2004.12.041.

McDonald, B. C. *et al.* (2018) 'Volatile chemical products emerging as largest petrochemical source of urban organic emissions', *Science*, 764(February), pp. 760–764.

Mckinney, K. A. *et al.* (2018) 'A sampler for atmospheric volatile organic compounds by copter unmanned aerial vehicles', *Atmospheric Measurement Techniques*, 12(September), pp. 3123–3135.

Millet, D. B. *et al.* (2008) 'Spatial distribution of isoprene emissions from North America derived from formaldehyde column measurements by the OMI satellite sensor', *Journal of Geophysical Research*, 113(D2), pp. 1–18. doi: 10.1029/2007JD008950.

Molina, M. *et al.* (2009) 'Reducing abrupt climate change risk using the Montreal Protocol and other regulatory actions to complement cuts in CO 2 emissions', *PNAS*, 106(49), pp. 20616–20621.

Mutius, E. Von *et al.* (1995) 'Air pollution and upper respiratory symptoms in children form East Germany', *European Respiratory Journal*, 8(5), pp. 723–728. doi: 10.1183/09031936.95.08050723.

Pagonis, D. *et al.* (2019) 'Autoxidation of Limonene Emitted in a University Art Museum', *Environmental Science & Technology Letters*. American Chemical Society, 6, pp. 520–524. doi: 10.1021/acs.estlett.9b00425.

Parker Hannifin (2015) *CTS Series Pump Data Sheet*.

Perez-Padilla, R., Schilmann, A. and Riojas-Rodriguez, H. (2010) 'Respiratory health effects of indoor air pollution', *The International Journal of Tuberculosis and Lung Disease*, 14(9), pp. 1079–1086.

Petrokofsky, G. *et al.* (2012) 'Comparison of methods for measuring and assessing carbon stocks and carbon stock changes in terrestrial carbon pools . How do the accuracy and precision of current methods compare ? A systematic review protocol', *Environmental Evidence*, 1:6, pp. 1–21.

Phalen, R. F. (2004) 'The particulate air pollution controversy', *Nonlinearity in Biology, Toxicology, and Medicine*, 2(4), pp. 259–292. doi: 10.1080/15401420490900245.

Place, C. *et al.* (2009) 'Assessment of Volatile Organic Compounds from Tubing Used for Soil Vapour Sample Collection Prepared by : CARO Analytical Services Submitted to : Science Advisory Board for Contaminated Sites in British Columbia Department of Chemistry University of Victoria PO Box 3064 Stn C', pp. 1–23.

Politzer, P., Murray, J. S. and Bulat, F. A. (2010) 'Average local ionization energy : A review', *Journal of Molecular Modeling*, 16, pp. 1731–1742. doi: 10.1007/s00894-010-0709-5.

RAE Systems (2013) *The PID Handbook*. doi: 10.4000/books.ifea.3652.

Redlich, C. A., Sparer, J. and Cullen, M. R. (1997) 'Sick-building syndrome', *The Lancet*, 349(9057), pp. 1013–1016.

Resonance Ltd. (2016) 'PID Kit VUV Light Sources', (705), pp. 10–13.

Robinson, E. and Robbins, R. C. (1970) 'Gaseous Nitrogen Compound Pollutants from Urban and Natural Sources Gaseous Nitrogen Compound Pollutants from Urban and Natural Sources', *Journal of the Air Pollution Control Association*, 20(5), pp. 303–306. doi: 10.1080/00022470.1970.10469405.

Sacks, J. D. *et al.* (2011) 'Review Particulate Matter – Induced Health Effects: Who Is Susceptible?', *Environmental Health Perspectives*, 119(4), pp. 446–454. doi: 10.1289/ehp.1002255.

Sandstrom, T. and Forsberg, B. (2008) 'Desert Dust: An Unrecognized Source of Dangerous Air Pollution', *Epidemiology*, 19(6), pp. 808–809. doi: 10.1097/EDE.0b013e31818809e0.

Schindler, D. W. (1999) 'The mysterious missing sink', *Nature*, 398(March), pp. 105–107.

Schraufnagel, D. E. *et al.* (2019) 'Air Pollution and Noncommunicable Diseases: A Review by the Forum of International Respiratory Societies ' Environmental Committee , Part 1 : The Damaging Effects of Air Pollution', *CHEST*. Elsevier Inc, 155(2), pp. 409–416. doi: 10.1016/j.chest.2018.10.042.

Schwartz, J. *et al.* (2005) 'Glutathione-S-Transferase M1, Obesity, Statins, and Autonomic Effects of Particles', *AMERICAN JOURNAL OF RESPIRATORY AND CRITICAL CARE MEDICINE*, 172(12), pp. 1529–1533.

Sevcik, J. (1976) 'Detectors in Gas Chromatography', *Journal of Chromatography*, 4(The Photoionization Detector), pp. 123–132.

Silva, R. A. *et al.* (2016) 'The Impact of Individual Anthropogenic Emissions Sectors on the Global Burden of Human Mortality due to Ambient Air Pollution', *Environmental Health Perspectives*, 124(11), pp. 1776–1784.

Simoni, M. *et al.* (2015) 'Adverse effects of outdoor pollution in the elderly', *Journal of Thoracic Disease*, 7(1), pp. 34–45. doi: 10.3978/j.issn.2072-1439.2014.12.10.

Spencer, R. C. (2003) 'Bacillus anthracis', *Journal of Clinical Pathology*, 56(3), pp. 182–187.

ter Steege, H. *et al.* (2013) 'Hyperdominance in the Amazonian Tree Flora', *Science*, 342(6156), pp. 325–342. doi: 10.1126/science.1243092.

Stewart, D. R. *et al.* (2017) 'Linking Air Quality and Human Health Effects Models: An Application to the Los Angeles Air Basin', *Environmental Health Insights*, 11, pp. 1–13. doi: 10.1177/1178630217737551.

Stober, A. K., Scolnik, R. and Hennes, J. P. (1963) 'A Vacuum Ultraviolet Photoionization Detector', *Applied Optics*, 2(7), pp. 735–740.

Tipler, P. (1987) *College Physics*. Worth Publishers.

Tuomi, T. *et al.* (2000) 'Emission of Ozone and Organic Volatiles from a Selection of Laser Printers and Photocopiers Emission of Ozone and Organic Volatiles from a Selection of Laser Printers and Photocopiers', *Applied Occupational and Environmental Hygiene*, 15(8), pp. 629–634. doi: 10.1080/10473220050075635.

United States EPA (2019) *Air Pollution: Current and Future Challenges*, *Clean Air Act Overview*.

Vennemo, H. *et al.* (2009) 'Environmental Pollution in China: Status and Trends', *Review of Environmental Economics and Policy*, 3(2), pp. 209–230. doi: 10.1093/reep/rep009.

Villa, T. F., Gonzalez, F., *et al.* (2016) 'An Overview of Small Unmanned Aerial Vehicles for Air Quality Measurements : Present Applications and Future Prospectives', *Sensors*, 16(1072), pp. 12–20. doi: 10.3390/s16071072.

Villa, T. F., Salimi, F., *et al.* (2016) 'Development and Validation of a UAV Based System for Air Pollution Measurements', *Sensors*, 16(12), pp. 1–15. doi: 10.3390/s16122202.

Wang, D. (2017) *Drone-Based VOC Sampling System for Atmospheric Insights in the Amazon*.

Wang, J. M. *et al.* (2015) ‘Plume-based analysis of vehicle fleet air pollutant emissions and the contribution from high emitters’, *Atmospheric Measurement Techniques*, 8(8), pp. 3263–3275. doi: 10.5194/amt-8-3263-2015.

Wang, W. *et al.* (2016) ‘Approaching the Truth of the Missing Carbon Sink’, *Polish Journal of Environmental Studies*, 25(4), pp. 1799–1802. doi: 10.15244/pjoes/62357.

Weinhold, B. (2008) ‘Ozone Nattion: EPA Standard Panned by the People’, *Environmental Health Perspectives*, 116(7), pp. 302–305.

Wennberg, P. O. *et al.* (2018) ‘Gas-Phase Reactions of Isoprene and Its Major Oxidation Products’, *Chemical Reviews*, 118, pp. 3337–3390. doi: 10.1021/acs.chemrev.7b00439.

Wiedinmyer, C. and Hurteau, M. D. (2010) ‘Prescribed Fire As a Means of Reducing Forest Carbon Emissions in the Western United States’, *Environmental Science & Technology*, 44(6), pp. 1926–1932.

Wilkins, E. T. (1954) ‘Air pollution aspects of the London fog of December 1952’, *Quarterly Journal of the Royal Meteorological Society*, 80(344), pp. 267–271.

Yamada, S., Hino, A. and Ogawa, T. (1984) ‘A highly sensitive laser two-photon ionization detector for liquid chromatography’, *Analytica Chimica Acta*, 156, pp. 273–277.

Zeng, Y. *et al.* (2019) ‘Air pollution reduction in China : Recent success but great challenge for the future’, *Science of the Total Environment*. Elsevier B.V., 663(24), pp. 329–337. doi: 10.1016/j.scitotenv.2019.01.262.

Zhang, H. and Ying, Q. (2011) ‘Contributions of local and regional sources of NOx to ozone concentrations in Southeast Texas’, *Atmospheric Environment*. Elsevier Ltd, 45(17), pp. 2877–2887. doi: 10.1016/j.atmosenv.2011.02.047.

Zhang, J. J. and Smith, K. R. (2003) ‘Indoor air pollution : a global health concern’, *British Medical Bulletin*, 68(1), pp. 209–225. doi: 10.1093/bmb/ldg029.

Zhou, Q. *et al.* (2018) ‘Development of a Novel Micro Photoionization Detector for Rapid Volatile Organic Compounds Measurement’, *Applied Bionics and Biomechanics*, 2018, p. 9.

8. APPENDIX: COMPONENTS USED

Part Name	Part Number	Vendor	Unit Price	Number of parts	Total price
Medium Power VUV PID Kit Exciter	PID-KMD-EX	Resonance Ltd.	$2512.00	1	$2512.00
Kr 12 mm Photovac 10.6 e.v. PID Bulb	KrLM-LPV	Resonance Ltd.	$309.00	1	$309.00
Super-Conductive 101 Copper Pipe	8965K33	McMaster—Carr	$28.05 per foot	1	28.05
Super-Conductive 101 Copper Rod	8965K71	McMaster—Carr	$29.25 per foot	1	$29.25
Brass Low-Pressure Barbed Tube Fitting	44555K113	McMaster—Carr	$2.34	6	$14.04
Borosilicate Glass Rod	8496K2	McMaster—Carr	$3.37	1	$3.37
PTFE Bar 1/4" Thick, 3" Wide	8735K76	McMaster—Carr	$53.40 per foot	1	$53.40
3M PTFE Thread Sealant Tape	4934A13	McMaster—Carr	$6.48	1	$6.48
5V Step-Up/Step-Down Voltage Regulator	S18V20F5	Pololu	$14.95	1	$14.95

Parker CTS 5-volt micro diaphragm pump	E164-11-050	Parker Hannifin	$159.00	1	$159.00
Raspberry Pi 3 Complete Starter Kit	4328435117	CanaKit via Amazon	$64.99	1	$64.99
EN3 3-Position Female Plug	EN3C3FX	Switchcraft Inc. via Digikey	$7.64	1	$7.64
PTFE Semi-Clear Tubing 1/4" ID 5/16" OD	5239K13	McMaster—Carr	$11.35	1	$11.35
Aluminum Oxide Rods	3 mm diameter, 32 mm long	Cemanco	$0.00 (donation)	5	$0.00
Female to Female Jumper Wires	4330127279	GenBasic via Amazon	$5.99	1	$5.99
PTFE Bar 1/2" Thick, 1-1/2" Wide	8735K38	McMaster—Carr	$53.40	1	$53.40
4A Step-Up DC-DC Converter	XL6009	Lee's Electronics	$11.40 (CA $15.00)	1	$11.40
XT30 Male & Female Connectors	B073WWWMQP	Crazepony via Amazon	$7.99	1	$7.99
XT60 Female Connector	B07BF8154S	Padarsey via Amazon	$6.99	1	$6.99

High Precision Raspberry Pi AD/DA Convertor	B00ZZGDL32	Waveshare via Amazon	$37.99	1	$37.99
Air Pressure Sensor	MPX4100AP	NXP USA Inc. via Digikey	$17.82	1	$17.82
Air Flow Sensor	HAFBLF0750CAAX5	Honeywell via Digikey	$78.81	1	$78.81
PTFE Semi-Clear Tubing 3/16" ID, 1/4" OD	5239K12	McMaster—Carr	$8.45	1	$8.45
Transfer Impedance Amplifier	Custom	Jim MacArthur	$129.85	1	$129.85
Total Material Costs:					**$3572.21**

Additionally, various fasteners (screws, washers, zip ties, tubing connectors, pipe clamps, ring terminals, etc.), acrylic sheets, electric components (various cables, breadboards), and PTFE rod used for bushings were provided by the Harvard Active Learning Laboratories, the Harvard Physics Machine shop, and/or the Martin Research Group. The DJI Matrice 600 Pro Hexacopter UAV belongs to the Martin Research Group. All testing equipment used belongs to either the Harvard Active Learning Laboratories, Harvard Physics Electronics Shop, or the Martin Research Group.